

Review

Solution coordination chemistry of actinides: Thermodynamics, structure and reaction mechanisms

Zoltan Szabó^a, Takashi Toraiishi^b, Valerie Vallet^c, Ingmar Grenthe^{a,*}

^a Department of Chemistry, Inorganic Chemistry, Royal Institute of Technology (KTH), Teknikringen 36, S-10044 Stockholm, Sweden

^b Department of Quantum Engineering and Systems Science, Graduate School of Engineering, University of Tokyo, 7-3-1 Hongo, Bunkyo-ku, 113-856 Tokyo, Japan

^c Laboratoire PhLAM, UMR CNRS 8523, Université des Sciences et Technologies de Lille, F-59655 Villeneuve d'Ascq, France

Received 31 July 2005; accepted 6 October 2005

Available online 4 January 2006

Contents

1. Introduction	785
2. Equilibrium analytical methods	785
2.1. Potentiometry	785
2.2. Spectroscopic methods	787
2.2.1. UV/vis spectrophotometry	787
2.2.2. Fluorescence (luminescence) spectrophotometry	788
2.2.3. To conclude	792
3. Limitations of the “classical” equilibrium analytical methods	792
4. Structure determination of complexes in solution	792
4.1. The structure of actinide aqua ions	793
4.1.1. The actinide(III) ions	793
4.1.2. Actinide(IV) ions	793
4.1.3. Actinyl(V) aqua ions	793
4.1.4. Actinyl(VI) aqua ions	794
4.2. The constitution and structure of actinide complexes ion solution	794
4.2.1. Actinide(III) complexes	794
4.2.2. Actinide(IV) complexes	795
4.2.3. Actinyl(V) complexes	795
4.2.4. Actinyl(VI) complexes	795
4.2.5. Coordination of multidentate ligands	796
5. The rate and mechanism of ligand substitution reactions	796
5.1. Mechanisms for water exchange in actinyl(V) and (VI) ions	798
5.2. Mechanisms for fluoride exchange in $UO_2F_n^{2-n}$ complexes	799
5.3. Mechanisms for fluoride exchange in ternary uranyl(VI) complexes	800
5.4. Chelate ring opening/ring closure reactions	801
5.5. Inter-molecular exchange between free and coordinated chelate ligands	804
5.6. Water exchange in uranyl(VI) complexes	805
5.7. Reaction mechanisms in actinyl(V) complexes	806
5.8. Reaction mechanisms in actinide(IV) and actinide(III) aquo ions	806
5.9. Entropy changes in chemical reactions	806
6. Ligands of biological interests	807
6.1. Amino acids, peptides	807
6.2. Nucleotides	809
6.3. Hydroxycarboxylates	811
Acknowledgements	813
References	813

* Corresponding author. Tel.: +46 87908144.

E-mail address: ingmarg@kth.se (I. Grenthe).

Abstract

The emphasis of this review is on the combination of experimental and theoretical methods to obtain microscopic information on the chemistry of actinides in aqueous solution. A brief discussion is given of some important experimental methods that provide information on the equilibrium constants and constitution of actinide complexes in solution, their structure and the rate and mechanism of ligand substitution reactions. The microscopic perspective is provided by a comparison of experimental data with those obtained using quantum chemical methods; the emphasis is here on structure and reaction mechanisms. Most of the experimental data refer to the chemistry of uranium, thorium and curium, but this information can be generalized to other actinides as their chemistry is often very similar in a given oxidation state. The first step in the analysis of complex formation in solution is based on equilibrium analytical methods; the discussion is here focused on those requiring macro amounts of actinides, as these are necessary in the methods used to obtain structure (large angle X-ray scattering, extended X-ray absorption spectroscopy and NMR) and dynamic (NMR, relaxation and stopped-flow methods) information. Finally, some comments are made on how the molecular understanding of complex formation between UO_2^{2+} and small ligands may be of importance in naturally occurring ligands like humic and fulvic acids and biomolecules, such as amino acids, proteins and nucleotides.

© 2005 Elsevier B.V. All rights reserved.

Keywords: Actinides; Solution coordination chemistry; Structure; Reaction mechanisms; NMR

1. Introduction

The emphasis of this review is on experimental methods that in combination with quantum chemical techniques can be used to obtain microscopic information on the chemistry of actinides in aqueous solution. “Classical” chemical thermodynamics cannot provide such information by itself; it can only be used for empirical correlations of thermodynamic data with molecular concepts. However, quantum chemistry in combination with statistical thermodynamics starts with microscopic models and then uses these to calculate macroscopic properties that can be compared with experiments. We will discuss general principles, rather than giving a data compilation of which there is abundance.

The general problems dealt with in the solution coordination chemistry of the actinides are the same as in other fields of chemistry: to determine the constitution and equilibrium constants of complexes including the identification of isomers, i.e. chemical analysis, to determine their structure and to discuss chemical bonding and reactivity. We will not discuss the technical details in the quantum chemical methods but only use their results; in a recent review, we have given a technical discussion of some of the important problems encountered when using quantum chemical methods on actinide systems [1].

Any study of a chemical system must begin with a determination of its composition, be it pure phases or solution systems. The analytical methods depend on the system characteristics and those used to study equilibrium systems are very different from the ones for pure compounds, as briefly described in the following section.

2. Equilibrium analytical methods

Equilibrium analytical methods have been described by Rossotti and Rossotti [2] and more recently by Beck and Nagypál and Grenthe et al. [3]; all of them require the measurement of concentrations and accordingly result in the determination of concentration equilibrium constants. Concentrations can often be measured directly in spectroscopic methods, but not in poten-

tiometry. In the latter case it is necessary to ascertain that the activity of the ions participating in the reaction is proportional to their concentrations when their total concentration is varied. This is achieved by using an ionic medium, where an “inert” electrolyte that does not participate in the reaction under study is present in large excess. In this way the concentration equilibrium constants are true constants in the given ionic medium, however, with the provision that the activity coefficients of reactants and products are defined as unity in the given ionic medium and not at zero ionic strength. Comparison of concentration equilibrium constants in different ionic media requires the reference of a common standard state, usually the pure solvent, as described in Grenthe et al. [3, Chapter IX].

We will demonstrate the use of two methods, potentiometry and spectroscopic methods; Rossotti and Rossotti [2] give a more detailed and complete discussion of these and other methods. The potentiometric method will be demonstrated by the hydrolysis of Th(IV), while a more general discussion is made of the spectroscopic methods. We will not discuss liquid–liquid extraction and ion-exchange methods that both have found extensive use when studying actinide systems at trace concentration level; both are extensively described in Ref. [2].

2.1. Potentiometry

Potentiometric methods involve either the measurement of the free metal ion concentration using a metal-ion selective electrode or the measurement of the free ligand concentration. The latter can be measured either directly using a ligand specific electrode or indirectly using pH measurements when the ligand is a weak protolyte. For actinides the free metal ion concentration can only be measured using reversible redox couples, $\text{An}^{3+}/\text{An}^{4+}$ and $\text{AnO}_2^+/\text{AnO}_2^{2+}$. For the special case of uranium one can also obtain reproducible redox potentials for the $\text{UO}_2^{2+}/\text{U}^{4+}$ couple because a sufficiently large amount of UO_2^+ is present as a mediator for the electron transfer at the inert electrode, thereby ensuring stable electrode potentials [4]. Most potentiometric determinations of equilibrium constants have been made using measurement of the free ligand concentration, in general

using pH measurements; some studies of fluoride complexes have been made using a fluoride selective membrane electrode.

Metal ions are solvated and the coordinated water is a much stronger acid than the water solvent. Using Th(IV) as an example, hydrolysis reactions should therefore be formulated as¹



However, this reaction is more commonly written as



Eqs. (1) and (2) are shorthand notations to describe several simultaneous and rapid equilibrium reactions. W is the number of water ligands in the first coordination sphere of the metal ion. This value is sometimes known from structure determinations, as will be discussed in Section 4; for Th^{4+} , W is equal to 9 ± 1 .

The stoichiometry and equilibrium constants for reaction (1) are determined from the known analytical total concentrations of Th, Th_{tot} , and protons, H_{tot} , in different test solutions, together with an experimental determination of the free hydrogen ion concentration, $-\log_{10}[\text{H}^+]$. The following equations are used, where \bar{n}_{OH} denotes the average number of coordinated OH^- per Th(IV), equal to the number of protons released per Th(IV) in Eq. (1). $\beta_{n,m}$ denotes the equilibrium constant for reaction (1); H_{tot} is often a negative quantity.

$$\begin{aligned} \text{Th}_{\text{tot}} &= [\text{Th}^{4+}] + \sum m[\text{Th}_m(\text{OH})_n] \\ &= [\text{Th}^{4+}] + \sum \frac{m^* \beta_{n,m} [\text{Th}^{4+}]^m}{[\text{H}^+]^n} \end{aligned} \quad (3)$$

$$\begin{aligned} H_{\text{tot}} &= [\text{H}^+] - \sum n[\text{Th}_m(\text{OH})_n] \\ &= [\text{H}^+] - \sum \frac{n[\text{Th}^{4+}]^m}{[\text{H}^+]^n} \end{aligned} \quad (4)$$

$$\bar{n}_{\text{OH}} = \frac{[\text{H}^+] - H_{\text{tot}}}{\text{Th}_{\text{tot}}} \quad (5)$$

If \bar{n}_{OH} is independent of Th_{tot} the system is mononuclear, if not polynuclear complexes are formed. To determine the stoichiometry of the complexes and the equilibrium constants in the system, it is necessary to vary the total concentration Th_{tot} and $-\log[\text{H}^+]$ over as large a range as possible, but in this example this is limited by the low solubility of thorium hydrous oxides. It is not possible to decrease the total concentration below approximately 0.1 mM, because protolytic impurities in the ionic medium will then result in a large error in \bar{n}_{OH} . For reasons of accuracy, the $-\log_{10}[\text{H}^+]$ range is limited to values above 2.5; the upper limit is given by the onset of precipitation of thorium hydroxide/hydrous oxide at about $-\log[\text{H}^+] = 4$, depending on the Th concentration.

¹ In cases where one does not know the origin of the released hydrogen ions one often uses the following notation; some charges are omitted for simplicity: $m\text{M} + n\text{H}_2\text{O} \rightleftharpoons \text{M}_m\text{H}_{-n} + n\text{H}^+$; for Th(IV) the protons may derive from coordinated water or coordinated hydroxide.

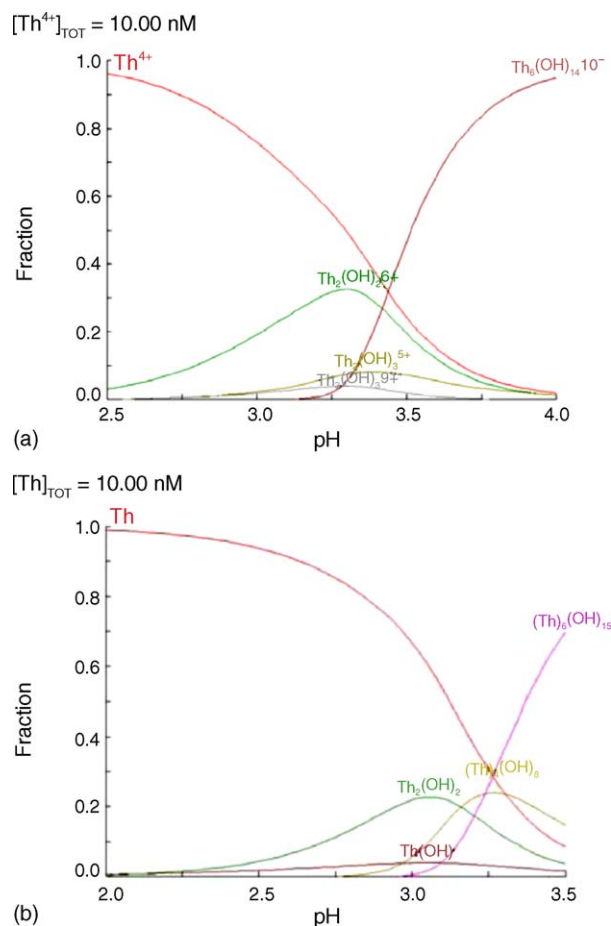


Fig. 1. (a) Distribution diagram for the Th(IV)–hydroxide system in 3 M NaCl, using the “best” set of equilibrium constants from Model 3B in Table 1. Note that many of the complexes suggested there occur in so low concentrations that they are not seen in the figures. (b) Distribution diagram for the Th(IV)–hydroxide system from data in 1 M NaClO₄ using data re-analyzed by Hietanen and Sillén [5].

Rossotti and Rossotti [2] summarize the various methods to deduce equilibrium constants from experimental data. In current practice graphical methods have been replaced by least-squares methods where the calculated data for different chemical models, in the example \bar{n}_{OH} versus $-\log[\text{H}^+]$, are tested against the experimental data. The chemical model where the agreement between experimental and calculated data is within the estimated experimental uncertainty and has the smallest least-squares residual, is selected as the “best” one. The analysis of experimental data is not an exercise in applied mathematics and chemical insight is essential, if this is not used one may easily draw erroneous chemical conclusions, as will be demonstrated by the Th-example. Fig. 1 shows a speciation diagram of the concentrations of the different Th–hydroxide complexes as a function of $-\log[\text{H}^+]$ based on equilibrium constants deduced by Hietanen and Sillén [5] from experimental data in a 3 M NaCl ionic medium. Table 1 describes the various models tested and the “best” one has been chosen using statistical criteria alone. It is noticeable that all models give a good description of the experimental observations. Several of the suggested species

Table 1

The “best” combinations of equilibrium constants for Th(IV) hydrolysis in 3 M NaCl [5] as identified by a LETAGROP least-squares analysis; the complexes $\text{Th}_m(\text{OH})_n^{4m-n}$ are denoted $n:m$

$n:m$	Model 1A	Model 1B	Model 2A	Model 2B	Model 3A	Model 3B	Model 3'A	Model 4A	Model 4B
1:1	-4.60 ± 0.20	-4.52 ± 0.13	-4.77 ± 0.18	-4.57 ± 0.13	-5.23	-5.14 ± 0.22	-5.28	-5.04 ± 0.25	-4.97 ± 0.16
1:2	-	-	-	-	-	-	-2.64	-	-
2:2	-4.83 ± 0.08	-4.90 ± 0.06	-4.74 ± 0.06	-4.90 ± 0.08	-4.75 ± 0.05	-4.78 ± 0.04	-4.78 ± 0.06	-4.74 ± 0.05	-4.76 ± 0.04
3:2	-	-	-9.14	-8.68 ± 0.12	-8.71 ± 0.10	-8.72 ± 0.08	-8.67 ± 0.10	-8.93	-8.94 ± 0.20
5:2	-	-	-	-	17.32	-17.16 ± 0.14	-17.39	-17.09 ± 0.18	-16.99 ± 0.11
1:3	-	-	-	-	-1.35 ± 0.23	-1.50 ± 0.23	-	-1.19 ± 0.19	-1.36 ± 0.18
2:3	-4.05	-	-3.92 ± 0.24	-4.53	-	-	-	-	-
3:3	-	-	-	-	-6.90 ± 0.20	-6.86 ± 0.14	-6.92 ± 0.23	-6.86 ± 0.19	-6.83 ± 0.13
8:4	-20.97	-	-	-	-	-	-	-21.06	-21.11 ± 0.22
9:4	-24.26 ± 0.11	-24.22 ± 0.08	-	-	-	-	-	-	-
11:5	-	-	-28.56 ± 0.10	-29.61	-	-	-	-	-
12:5	-	-	-32.56 ± 0.13	-32.24 ± 0.10	-	-	-	-	-
14:6	-	-	-	-	-36.38 ± 0.04	-36.42 ± 0.03	-36.38 ± 0.04	-36.56 ± 0.13	-36.58 ± 0.10
25:10	-	-	-	-	-	-	-	65.29	-65.35 ± 0.21
$\sigma(\bar{n}_{\text{OH}})$	0.044	0.030	0.023	0.014	0.015	0.011	0.016	0.013	0.010

Model 1 has $m \leq 4$, Model 2 has $m \leq 5$, Model 3 $m \leq 6$ and Model 4 no restrictions on m . In Models A no systematic errors are taken into account; in Models B the least-squares refinements have been made by assuming a systematic error in \bar{n}_{OH} . The standard deviation $\sigma(\bar{n}_{\text{OH}})$ is small but systematically smaller for the models with $m \leq 6$; these accordingly represent the “best” set of those investigated. Complexes that are poorly defined in the least-squares analysis have no estimated standard deviation in $\log_{10} \beta_{n,m}$.

occur in very low concentration and some of their proposed stoichiometries make little chemical sense, e.g. $\text{Th}_3(\text{OH})^{11+}$. Complexes that occur in small amounts may be artifacts that represent methodological shortcomings rather than real chemical species. To spot such artifacts it is necessary to use the deduced equilibrium constants to determine the concentrations of the different species in the test solutions. In addition to the mathematical/statistical analysis of the data one must also test if the proposed stoichiometry is consistent with the known coordination chemistry of the metal ion and ligand and other chemical insights. It is also wise to use the “Occam’s razor” principle and select the simplest model consistent with the experimental observations.

The mass balance equations (3) and (4) indicate that species in low concentrations are very prone to systematic experimental errors, such as protolytic impurities. This is a typical feature of all experimental methods where the experimental data are interpreted using a composite quantity like \bar{n}_{OH} .

Th(IV) hydrolysis has been studied in different ionic media and one expects that the same species should be present in all of them. Hietanen [6], Hietanen and Sillén [5] and Kraus and Holmberg [7] have studied hydrolysis of Th(IV) in 1 M NaClO_4 and presented equilibrium models that are significantly different from those in 3 M NaCl; these different speciation models are hard to reconcile with the fact that both perchlorate and chloride form no, or very weak, complexes with Th^{4+} . The experimental data of Hietanen and Sillén [5] in 3 M NaCl have later been reinterpreted by Baes and Mesmer [8] using a model that includes only three species $\text{Th}_2(\text{OH})_2^{6+}$, $\text{Th}_2(\text{OH})_3^{5+}$ and $\text{Th}_6(\text{OH})_{14}^{10+}$, species that are also prominent in 1 M NaClO_4 media (cf. Fig. 1b). However, note the slight difference in composition of the hexanuclear complex, $\text{Th}_6(\text{OH})_{14}^{10+}$, in 3 M NaCl and $\text{Th}_6(\text{OH})_{15}^{9+}$ in 1 M NaClO_4 .

2.2. Spectroscopic methods

Actinide ions are in general colored and some of them have fluorescence properties; these spectral characteristics depend on the chemical composition of the first coordination sphere and can accordingly be used to obtain information on chemical speciation. We will discuss three methods: spectrophotometry using the changes in the UV/vis spectra, measurements of fluorescence/luminescence properties and NMR spectroscopy. In the first two cases we will focus on the properties of the metal ion, even if measurements on the ligand also provide useful information. As examples we will use uranyl(VI) and Cm(III) complexes. The NMR method will be demonstrated by uranyl(VI) and Th(IV) complexes containing ligands with NMR active nuclei such as ^{13}C , ^{17}O and ^{19}F .

2.2.1. UV/vis spectrophotometry

In these experiments the absorbance is measured as a function of the total concentrations of reactants. To simplify the notation we delete charges and assume that only two mononuclear complexes are formed. The mass balance and measured absorbance are then equal to

$$\begin{aligned} M_{\text{tot}} &= [\text{M}] + [\text{ML}] + [\text{ML}_2] \\ &= [\text{M}](1 + \beta_1[\text{M}][\text{L}] + \beta_2[\text{M}][\text{L}]^2); \end{aligned} \quad (6)$$

$$A = \varepsilon_0[\text{M}] + \varepsilon_1[\text{ML}] + \varepsilon_2[\text{ML}_2]; \quad (7)$$

M_{tot} and A are the total concentration of the metal ion and the measured absorbance, respectively, ε_0 , ε_1 and ε_2 the molar absorptivity of metal ion and complexes (one can often find wave-length regions where the absorptivity of the ligand is negligible) and β_1 and β_2 are the equilibrium constants for the

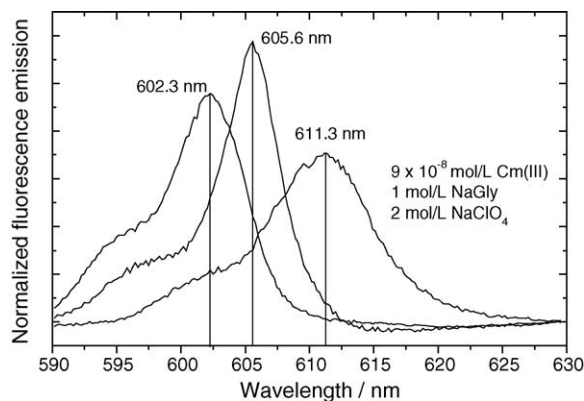


Fig. 2. The fluorescence emission spectra from the Cm–glycolate system (from Stumpf et al. [9], reproduced by the permission of the Royal Society of Chemistry), where the spectra for three different complexes have been obtained by peak deconvolution of composite spectra; spectra are scaled to the same peak area.

formation of ML and ML₂. From Eqs. (6) and (7) we have

$$\frac{A}{M_{\text{tot}}} = A_M = \frac{\varepsilon_0 + \varepsilon_1\beta_1[L] + \varepsilon_2\beta_2[L]^2}{1 + \beta_1[L] + \beta_2[L]^2}. \quad (8)$$

In addition to the equilibrium constant, one has to determine the molar absorptivity, ε , for each species; in fluorescence/luminescence spectroscopy the molar emissivity of each fluorescent species and in NMR spectroscopy the scaling factor between concentration and peak integrals (this has the same value for all species) for each species containing an NMR active element. The ease with which this can be accomplished varies strongly. Peak deconvolution can be used if the absorption/emission bands of the different species are well separated and provides direct information on the number of species formed; this is the situation in many fluorescence spectra as exemplified by Fig. 2, showing the fluorescence spectrum of a Cm(III)–glycolate system. This situation is also at hand in many NMR spectra, e.g. the ¹⁹F NMR spectrum of the ternary system UO₂²⁺–acetate[−]–F[−] shown in Fig. 3.

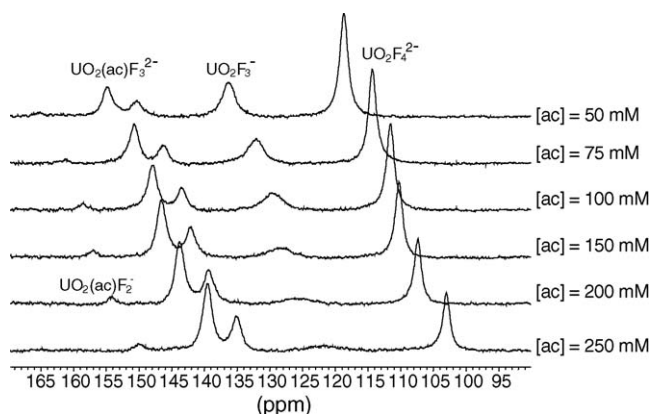


Fig. 3. ¹⁹F NMR spectra (from Aas et al. [10], reproduced by the permission of the Royal Society of Chemistry) of different test solutions in the UO₂²⁺–acetate[−]–F[−]. The peak integrals give direct information on the concentration of the different species.

It is often straightforward to determine the ε -values for the different species when deconvolution can be made and this information gives a direct measure of their concentration. This is a great advantage compared to the potentiometric method where these concentrations must be deduced from mass balance equations, with a resulting poor accuracy of the concentration of minor species. The molar absorptivity can vary strongly within a given system as exemplified by the uranyl(VI)–hydroxide system, where the molar absorptivity of the two- and three-nuclear complexes is very high as compared to UO₂²⁺. Their contribution to the measured absorptivity is thus large, a fact that improves the accuracy of the corresponding equilibrium constants. It is difficult to determine the individual molar absorptivities if the corresponding absorption bands overlap strongly; this is often the case for the UV/vis spectra of trivalent actinides.

Rossotti and Rossotti [2] give an exhaustive description how to analyze spectroscopic data, but there are also more recent methods described, e.g. by Lubal and Havel [11,12] and Meinrath et al. [13,14]. In many experimental studies of actinide complexes using spectroscopic methods, the experimental conditions have been arranged so that one equilibrium is predominating. For this case Eq. (8) is reduced to

$$A_M - \varepsilon_0 = \frac{\varepsilon_1\beta_1[L] - \varepsilon_0\beta_1[L]}{1 + \beta_1[L]}, \quad (9)$$

or

$$\frac{1}{A_M - \varepsilon_0} = \frac{1}{\varepsilon_1 - \varepsilon_0} + \frac{1}{\beta_1(\varepsilon_1 - \varepsilon_0)[L]}; \quad (10)$$

the equilibrium constant can then be determined graphically. From both Eqs. (8) and (10) it is obvious that the concentration of free ligand can only be determined if the complexes formed are not too strong. When strong complexes are formed it is necessary to determine the concentration of free ligand using a separate method, e.g. by measuring the pH if the ligand is a weak protolyte. The determination of equilibrium constants for uranyl(VI) and Cm(III) complexes using fluorescence spectroscopy requires very low metal ion concentrations and one can then calculate the free ligand concentration from the ligand mass balance without taking the amount coordinated to the metal ion into account.

2.2.2. Fluorescence (luminescence) spectrophotometry

Fluorescence (luminescence) spectrophotometry is an extensively used technique to study chemical equilibria. Since it has a very low detection limit, the analysis can be made at very low actinide concentrations. Several actinides such as U(VI) or Cm(III) have a characteristic long-lived luminescence, that is strongly influenced by the coordination of ligands, providing additional quantitative information on the complex formation. The peaks in the luminescence spectra of Cm(III) show relatively large shifts when complexes are formed and can therefore easily be separated from the signal of free Cm³⁺ using peak deconvolution (cf. Fig. 2). Kim et al. [15] used luminescence spectrophotometry to study the complexation of Cm(III) by carbonate. The well-separated spec-

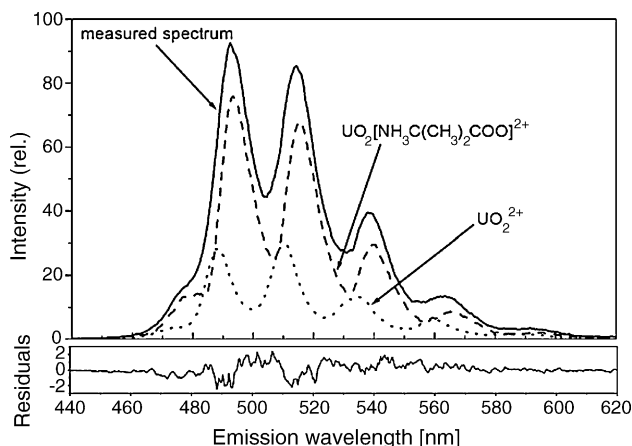


Fig. 4. Fluorescence spectrum from a test solution in the uranyl(VI) α -aminoisobutyrate system. The full-drawn curve is the measured spectrum and the dotted and dashed lines the deconvoluted spectra of UO_2^{2+} and $\text{UO}_2(\text{NH}_3^+\text{C}(\text{CH}_3)_2\text{COO}^-)^{2+}$; the inset shows the residuals between the measured spectrum and the sum of the deconvoluted spectra (from [24], reproduced by permission of *Radiochim. Acta*).

tra belonging to free Cm^{3+} and the different carbonate complexes allowed a direct determination of the concentration of each complex and their equilibrium constants. The same type of analysis was employed to study the Cm(III)–hydroxide, 5-sulfosalicylate, fluoride, chloride and glycolate systems [16–20].

The peaks in the luminescence spectra of U(VI) are rather broad (cf. Fig. 4), with often small peak shifts, resulting in a more complicated deconvolution. However, these difficulties can be surmounted and luminescence spectroscopy has been used to determine equilibrium constants in U(VI) systems with inorganic and organic ligands such as carbonate, sulfate, silicate and α -aminoisobutyrate [21–24]. The characteristics of the luminescence spectra of curium(III) and uranyl(VI) are shown in Figs. 2 and 4.

In systems where deconvolution is not possible, one may use time-resolved luminescence methods; an example is the study of complex formation in the U(VI)–silicate and U(VI)– α -aminoisobutyrate systems by Moll et al. [23,24]. They found that the complexes $\text{UO}_2\text{OSi}(\text{OH})_3^+$ and $\text{UO}_2(\text{NH}_3^+\text{C}(\text{CH}_3)_2\text{COO}^-)^{2+}$ could not be separated by deconvolution from UO_2^{2+} . However, the rate of fluorescence decay obtained from time-resolved spectra was bi-exponential, indicating the co-existence of two different chemical components with separate lifetimes. The difference between $\text{UO}_2^{2+}(\text{aq})$ and $\text{UO}_2(\text{NH}_3^+\text{C}(\text{CH}_3)_2\text{COO}^-)^{2+}$ is large, 1600 and 330 μs , respectively, and the luminescence spectra can be separated using time-gating. However, the determination of equilibrium constants using this method should be used with caution, since the chemical reaction in the excited state (vide infra) is also involved in the de-excitation process. If this is the case the equilibrium constant is different from the one in the ground state, as discussed by Billard and Lützenkirchen [25] using the “double-complexation” Scheme 1 in the ground and excited states.

The equilibrium constants in ground and excited states are defined as follows:

$$K = \frac{[\text{ML}(t)]}{[\text{M}(t)][\text{L}]} \quad (11a)$$

$$K^* = \frac{[\text{M}^*\text{L}(t)]}{[\text{M}^*(t)][\text{L}]} \quad (11b)$$

The time dependence of the luminescence is:

$$\frac{d}{dt}[\text{M}^*(t)] = -\{\lambda_1 + k_1[\text{L}]\}[\text{M}^*(t)] + k_{-1}[\text{M}^*\text{L}(t)] \quad (12a)$$

$$\frac{d}{dt}[\text{M}^*\text{L}(t)] = -\{\lambda_2 + k_{-1}\}[\text{M}^*\text{L}(t)] + k_1[\text{L}][\text{M}^*(t)] \quad (12b)$$

Integration gives:

$$[\text{M}^*(t)] = A \exp(\Lambda_+ t) + B \exp(\Lambda_- t) \quad (13a)$$

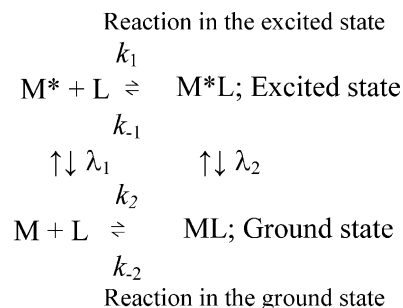
$$[\text{M}^*\text{L}(t)] = C \exp(\Lambda_+ t) + D \exp(\Lambda_- t) \quad (13b)$$

where

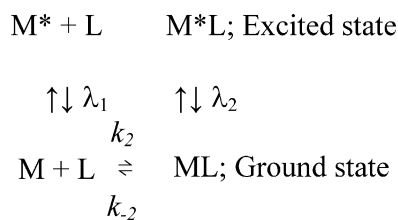
$$\Lambda_{\pm} = -\frac{1}{2}(\lambda_1 + \lambda_2 + k_1[\text{L}] + k_{-1}) \pm \frac{1}{2} \sqrt{(\lambda_1 + \lambda_2 + k_1[\text{L}] + k_{-1})^2 - 4(\lambda_2 + k_{-1})(\lambda_1 + k_1[\text{L}] - k_1 k_{-1}[\text{L}])} \quad (14)$$

Billard and Lützenkirchen have used Scheme 1 and the relationships (13a) and (13b) to deduce rate constants k_1 and k_2 from the amplitude of the emission spectra and ground state concentrations. These data provide information on ground state and excited state chemistry. The conclusion from their mathematical simulation was that the luminescence spectra could only be used for the determination of ground state equilibrium constants when k_1 and $k_{-1} \ll \lambda_1$ and λ_2 (Case I), but not when k_1 and $k_{-1} \sim \lambda_1$ and λ_2 (Case II) or when k_1 and $k_{-1} \gg \lambda_1$ and λ_2 (Case III). In Case I, the complex formation in the ground state can be neglected and Scheme 2 is a good approximation for Scheme 1.

In Scheme 2, the observed decay curve follows a pure bi-exponential function that does not depend on the concentration of any chemical component in the system, and the equilibrium constant is $K = K_{\text{app}}$, where K_{app} is directly evaluated from the



Scheme 1. A typical “double-complexation” reaction scheme after excitation. The chemical exchange reaction in the excited state controls the apparent luminescence decay [25], where k_1/k_{-1} and k_2/k_{-2} are the rate constants for the formation and dissociation of ML^* and ML , respectively, and λ_1 and λ_2 the rate constants for decay of M^* and ML^* .



Scheme 2. The reaction scheme when complex formation in the excited state is neglected.

luminescence intensity of the deconvoluted signals. This condition is fulfilled in the studies by Moll et al. [23,24] and in a study of the $\text{UO}_2^{2+}\text{-SO}_4^{2-}$ system by Geipel et al. [21], as confirmed by the numerical calculation by Billard and Lützenkirchen. In Case II, Eqs. (12a)–(14) describe the time-dependence of the luminescence. When there is mixing in the excited state, the intrinsic lifetimes belonging to M^* or M^*L are no longer equal to the experimental values λ_1 and λ_2 , even though the decay curve remains bi-exponential. This mixing also contributes to the luminescence intensity of each component [25]. If this is not considered the result will be an erroneous interpretation of the luminescence spectra and an erroneous equilibrium constant. Cases I and II can be distinguished from the $[\text{L}]$ dependence of the lifetime: in Case I, the experimental lifetime is equal to the intrinsic one and therefore does not depend on $[\text{L}]$, while in Case II, it is a function of $[\text{L}]$ (cf. Eqs. (12a) and (12b)). This concentration dependence must be checked before any analysis of the luminescence data can be made. In systems corresponding to Case II, the equilibrium constants are no longer obtained directly from the luminescence intensity, one has to use a numerical treatment together with the experimental data to deduce them. In Case III, the chemistry in the excited state becomes the dominating process and the measured equilibrium constant, K_{app} , refers to the excited state instead of the ground state. With some approximations we have

$$K_{\text{app}} = K^* \frac{\alpha \tau_1}{\beta \tau_2} \quad (15)$$

where K_{app} is the apparent equilibrium constant obtained from the deconvoluted luminescence spectra, α and β the molar absorption coefficients and τ_1 and τ_2 are the lifetimes of M^* and M^*L . In this case the observed lifetime often shows a mono-exponential decay when the concentration $[\text{L}]$ is relatively high, even though two different luminescent components are present in the spectra; the equilibrium constant in the ground state can then not be determined, as discussed by Moulin et al. [26] in their analysis of the $\text{UO}_2^{2+}\text{-OH}^-$ system. If the assumption $K^* \sim K$ is correct, the equilibrium constant in the ground state can be evaluated, but this is never guaranteed; the only case where the approximation is justified seems to be in the case of 4f-elements. The reason is that the 4f-electrons, which dominate the photo-excitation process, are not involved in the chemical reactions [27]. From the broad survey of different experimental studies, Billard and Lützenkirchen [25] conclude: U(VI) systems always correspond to Case I or II, with the exception of the $\text{UO}_2^{2+}\text{-F}^-$ system [28] that belongs to Case III. However, even this exception has been questioned; a “Round-robin” test by

several research groups concluded that the $\text{UO}_2^{2+}\text{-F}^-$ system probably shows multi-exponential decay [29]. The luminescence properties of all studied Cm(III) systems with inorganic ligands classify them to Case III, and some systems with organic ligand to Case II [21].

The equilibrium constant of U(VI) complexes may safely be obtained using luminescence spectroscopy, provided that the necessary numerical methods are used in Case II. However, for Cm(III) the experimental equilibrium constants determined from the luminescence intensity correspond to the reaction in the excited state, not to the ground state; great care should therefore be taken when interpreting the experimental results.

The coordination of a ligand often changes the luminescence quantum yield, which results in quenching or enhancement of the apparent luminescence intensity. For instance, in some of U(VI) complexes with organic ligands, the quantum yield is very close to zero [24,30] and the concentration of non-coordinated UO_2^{2+} in the aqueous phase can then be determined from the luminescence intensity using the relationship

$$\frac{[\text{M}]}{M_{\text{tot}}} = \frac{I}{I_0} \quad (16)$$

where $[\text{M}] = [\text{UO}_2^{2+}]$ and M_{tot} the total concentration of UO_2^{2+} ; I and I_0 refer to the luminescence intensity in the presence and absence of the ligand, respectively. The equilibrium constants can then be calculated in the same way as in potentiometric methods where the free metal ion concentration is measured by using a metal selective electrode [2]. For the simple case where a single complex ML is formed



we have

$$\begin{aligned}
 K &= \frac{[\text{ML}]}{[\text{M}][\text{L}]} = \frac{M_{\text{tot}} - [\text{M}]}{[\text{M}]} \frac{1}{\{L_{\text{tot}} - (M_{\text{tot}} - [\text{M}])\}} \\
 &= \frac{1 - I/I_0}{I/I_0} \frac{1}{\{L_{\text{tot}} - M_{\text{tot}}(1 - I/I_0)\}}. \quad (18)
 \end{aligned}$$

(I/I_0) is the only variable in Eq. (18) and provides direct information on the equilibrium constant from the measured luminescence intensity. If the experiment is made in the presence of a large excess of ligand, the concentration of free ligand is nearly constant and $[\text{L}] \cong L_{\text{tot}}$. Eq. (18) is then transformed to

$$K = \frac{1 - (I/I_0)}{(I/I_0) \cdot L_{\text{tot}}} \quad (19)$$

Hence,

$$\left(\frac{I}{I_0}\right)^{-1} = 1 + K \cdot L_{\text{tot}}. \quad (20)$$

This is the well-known Stern–Volmer equation; the plot of $(I/I_0)^{-1}$ versus L_{tot} is linear with the intercept 1 and the slope K . Moll et al. [24] have used this method to study the complex formation between UO_2^{2+} and α -substituted carboxylates, after confirming that there was no luminescence from the different UO_2^{2+} complexes (Fig. 5).

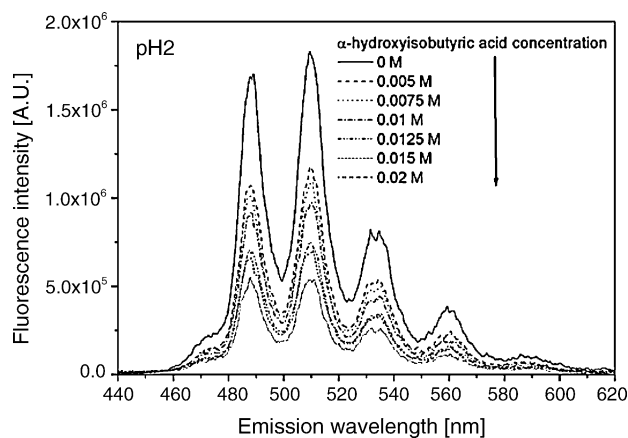


Fig. 5. The luminescence spectra in the uranyl(VI)– α -hydroxyisobutyrate system at pH 2 and a total uranyl(VI) concentration of 7×10^{-5} M, from Moll et al. [24] (reproduced by permission of *Radiochim. Acta*).

If complexes ML_n , $n > 1$, form, the ratio $(III_0)^{-1}$ (Eq. (20)) is no longer a linear function of L_{tot} , a fact that can be used to determine both the stoichiometry and the equilibrium constants of the various ML_n complexes, provided the free ligand concentration can be determined (at $M_{\text{tot}} \ll L_{\text{tot}}$, $[L] = L_{\text{tot}}$). By performing the experiments at different M_{tot} one can obtain information if polynuclear complexes are formed, or not. Measurements at different total concentrations of protons provide information on the possible occurrence of ternary complexes involving protons. In short, the analysis of solution chemical equilibria using fluorescence methods is completely analogous to those used in potentiometry.

The same method can also be used for fluorescent ligands, e.g. some aromatic ligands turn non-fluorescent on coordination to metal ions; III_0 can then be used to calculate the concentration of free ligand

$$\frac{[L]}{L_{\text{tot}}} = \frac{I}{I_0} \quad (21)$$

The determination of equilibrium constants using fluorescent ligands is made in the same way as for luminescent metal ions using Eqs. (17)–(20), but changing L_{tot} to M_{tot} and vice versa in Eqs. (18)–(20). This technique has the obvious advantage that it can be applied to “non-luminescent” actinides or other metal ion system. Examples on the use of ligand fluorescence is given by Toraiishi et al. that reported a detailed study of this type on the Ln(III)–salicylate system [31] and Geipel et al. [30] that studied the uranyl(VI)–2,5-dihydroxybenzoic acid system.

In order to obtain precise information on the stoichiometry and equilibrium constants using the procedure described above, two conditions must be satisfied: (1) the complex formation must be the only physical process that results in quenching of the luminescence and (2) the complexes formed must be non-fluorescent. However, in many cases both of these conditions are not satisfied. The latter condition can easily be checked from the shape of the luminescence spectra, while the former cannot be confirmed by analysis of the spectra alone. Time-resolved luminescence decay may offer an alternative when the effect of other quenching processes than complex formation can

be separated from the experimental luminescence quenching [31,32]. Several physical or chemical processes, e.g. collision with other molecules in the system (generally known as collisional quenching) and non-radiative exciplex formation in the excited state, are often lumped together and referred to as a “dynamic” process, described by a rate constant, k_q . For instance, the non-complexing ClO_4^- acts as a quencher for UO_2^{2+} luminescence by forming a non-luminescent exciplex in the excited state. Billard et al. have discussed details on this phenomenon [33]. The quenching caused by the formation of non-luminescent complexes in the ground state is often called “static” quenching to distinguish it from “dynamic” processes. The experimental luminescence lifetime, τ , is described by three de-excitation processes, emission, non-radiative decay and dynamic physical processes with rate constants Γ , k_{nr} and k_q , respectively. Because the depopulation from the lowest excited state is described by first-order rate equations for all three processes we have

$$\tau = \frac{1}{\Gamma + k_{\text{nr}} + k_q} \quad (22)$$

III_0 may depend on the fraction of excited species relative to the total, which decay by emission. $(III_0)^{-1}$ is given by the ratio of the decay rate in the absence of quencher, ($\gamma = \Gamma + k_{\text{nr}}$), to the total decay rate in the presence of quencher, ($\gamma + k_q[Q]$).

$$\left(\frac{I}{I_0}\right)^{-1} = \frac{\gamma + k_q[Q]}{\gamma} = 1 + \left(\frac{k_q}{\gamma}\right)[Q] = 1 + k_q\tau_0[Q] \quad (23)$$

Since dynamic quenching is a process which depopulates the excited state, the lifetimes in the absence (τ_0) and presence (τ) of quencher are given by

$$\tau_0 = \gamma^{-1} \quad (24)$$

$$\tau = (\gamma + k_q[Q])^{-1}, \quad (25)$$

and therefore

$$\left(\frac{\tau}{\tau_0}\right)^{-1} = \frac{\gamma + k_q[Q]}{\gamma} = 1 + k_q\tau_0[Q]. \quad (26)$$

Eqs. (23) and (26) provide an important characteristic of “dynamic” quenching:

$$\left(\frac{I}{I_0}\right)^{-1} = \left(\frac{\tau}{\tau_0}\right)^{-1}. \quad (27)$$

“Static” quenching takes place in the ground state and is not involved in relaxation pathways from the lowest excited state. If this is the only process, τ is constant, equal to τ_0 , and the relationship

$$\left(\frac{\tau}{\tau_0}\right)^{-1} = \text{constant} = 1 \quad (28)$$

should be satisfied. The variable $(\tau/\tau_0)^{-1}$ is evaluated from the time-resolved luminescence spectra, and the effect of “dynamic” quenching can be subtracted from the measured total luminescence quenching by using the relationship (27) [34].

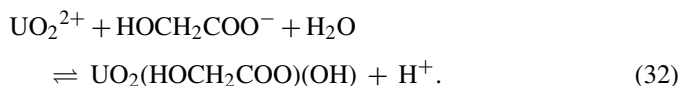
2.2.3. To conclude

The examples of the preceding sections demonstrate some of the characteristics of the experimental methods used in equilibrium analysis. The section is not exhaustive and only intends to demonstrate the characteristics of some important experimental methods. It is often necessary to use more than one method before proceeding with the subsequent “microscopic” analysis of the problem at hand. Care should be taken when discussing the chemical implications of complexes that are present in low concentrations according to the experimental data; they may be methodological artifacts. Fluorescence spectroscopy can be used in systems with very low total concentrations of actinides, and thereby offer an important advantage over other methods such as potentiometry and NMR spectroscopy.

Raman methods [35a,b] have been used to study carbonate complexes of actinyl(V) and (VI) carbonate complexes and the hydrolysis in the uranyl(VI) system, but the method requires fairly high actinide concentrations.

3. Limitations of the “classical” equilibrium analytical methods

Potentiometric and other “classical” equilibrium analytical methods cannot distinguish between the different origins of the protons released in hydrolysis reactions such as Eq. (1), or in systems where the complex formation takes place with ligands that are polyprotic acids where the protons may originate either from coordinated water/hydroxide or from the ligand; this so-called “proton ambiguity” is demonstrated by the following two examples:



In the same way the classical methods, with the exception of some spectroscopic methods, notably NMR, cannot distinguish between isomers that have the same stoichiometry. The experimental equilibrium constant for the formation of a complex ML, which may consist of different isomers, is then

$$\begin{aligned} K &= \frac{[\text{ML}]}{[\text{M}][\text{L}]} = \frac{[\text{ML}]_1 + [\text{ML}]_2 + [\text{ML}]_3 + \dots}{[\text{M}][\text{L}]} \\ &= K_1 + K_2 + K_3 + \dots, \end{aligned} \quad (33)$$

where $[\text{ML}]_1$ and $[\text{ML}]_2$ are the concentrations of the different isomers that all have the same stoichiometry; only the sum of these concentrations is obtained in the “classical” equilibrium determinations. Fig. 6 shows the ^{19}F NMR spectrum and peak assignments from a test solution where four different complexes have been identified, UO_2F^+ , $\text{UO}_2\text{F}_2(\text{aq})$, $\text{UO}_2(\text{oxalate})\text{F}_2^{2-}$ and $\text{UO}_2(\text{oxalate})\text{F}(\text{OH}_2)_2^-$. There are two different (broad)

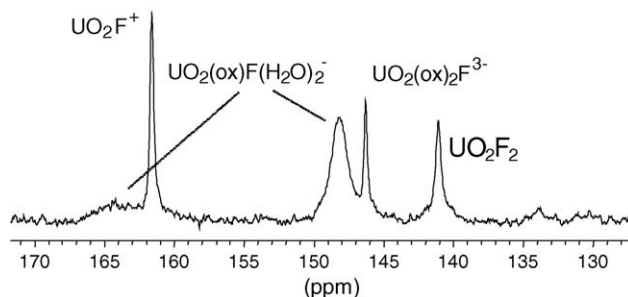


Fig. 6. The ^{19}F NMR spectrum of a test solution containing the complexes UO_2F^+ , $\text{UO}_2\text{F}_2(\text{aq})$, $\text{UO}_2(\text{oxalate})\text{F}_2^{2-}$ and $\text{UO}_2(\text{oxalate})\text{F}(\text{OH}_2)_2^-$ (from Szabó et al. [36], reproduced by the permission of American Chemical Society). The peak sizes indicate that the two isomers of $\text{UO}_2(\text{oxalate})\text{F}(\text{OH}_2)_2^-$ have different stability constants; Szabó et al. suggest that the smaller peak at 164 ppm refers to complex 2 and the larger peak at 147.5 ppm to complex 1.

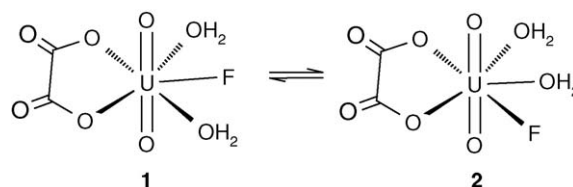


Fig. 7. Structures of the two possible isomers of $\text{UO}_2(\text{oxalate})\text{F}(\text{OH}_2)_2^-$ (from Szabó et al. [36], reproduced by the permission of American Chemical Society).

peaks for the latter complex demonstrating that there are two different isomers present; their structure is shown in Fig. 7.

It is important to consider these limitations in systems where the ligand contains many donor atoms and where different modes of coordination are possible. The magnitude of the equilibrium constants may be used as an indicator for the mode of coordination of a ligand, as exemplified by $\log \beta_1$ equal to 2.44 and 2.16, respectively, for the complexes UO_2L^+ , where L is acetate or glycolate. The fact that the glycolate complexes with two potential coordinating functional groups ($-\text{COO}^-$ and $-\text{OH}$) are weaker than the corresponding acetate complexes is a strong indication that the $-\text{OH}$ group is not coordinated. This qualitative type of reasoning has also been extended to the reaction enthalpy and reaction entropy, where the latter quantity has been assumed to be an indicator for the number of water ligands “set free” in complex formation reactions $\text{M}(\text{OH}_2)_N + n\text{L}(\text{aq}) \rightleftharpoons \text{M}(\text{OH}_2)_m\text{L}_n + (N - m)\text{H}_2\text{O}$; the charges have been omitted for simplicity. The high stability of chelate complexes is then seen as a result of the large number of water ligands that are replaced by the chelating ligand; Vallet et al. [37] have discussed the chelate effect in some detail.

4. Structure determination of complexes in solution

Structure information on complexes in solution can be obtained from spectroscopy (NMR, IR and Raman) that provides information on the mode of coordination of a certain ligand and the symmetry of complexes with ligands of known geometry. Large angle X-ray diffraction (LAXS) and extended X-ray absorption fine structure data (EXAFS) give structure

information in the form of radial distribution functions that are one-dimensional representations of the structures. The peaks in the functions provide information on the distances between pairs of atoms and their intensity information on the number of these distances. LAXS data provide information on all pair distances, but pairs that contain heavy atoms such as actinides dominate the intensity. It is often difficult to determine the pair distance between light atoms like oxygen, unless there are many of them. The radial distribution function in EXAFS provides information on bond distances between a specific “target” atom, in this case the actinide, and distances to other atoms in surrounding “shells”. The bond distance is an average and the distribution around this average depends on the amplitude of the vibrational movement of the atoms (the Debye–Waller factor), but not on the rate of ligand exchange, as this is much slower than the “interaction time” between the incident X-ray quanta and the atom electrons.

The accuracy of bond distances is in general about 0.02 Å in both methods, but the determination of the number of a certain bond distance is much less precise, especially in EXAFS. Hence, the error in the coordination number is in general is large, 10–20%. The bond distances provide a first guide on the mode of coordination of a certain ligand, but comparison with models is needed to select a proper three-dimensional structure. Reviews by Johansson [38] and Den Auwer et al. [39] give more details on the methodology.

The combination of LAXS/EXAFS data with quantum chemical methods is a powerful tool for the elucidation of the three-dimensional structure of complexes in solution as discussed in recent reviews by Vallet et al. [1,40].

4.1. The structure of actinide aqua ions

4.1.1. The actinide(III) ions

The only direct structure information on the solution structures of the actinide(III) aqua ions has been provided by XANES [41] data in combination with quantum chemical calculations [41,42] and EXAFS [43,44]. The experimental coordination number for $\text{Pu}^{3+}(\text{aq})$ from the EXAFS data is 10 ± 1 , while quantum chemical calculations [42] give values of 8 or 9. Experimental and calculated $\text{Pu}^{3+}\text{--OH}_2$ distances agree fairly well, 2.51 Å

versus 2.55 Å for nine-coordination [42]. The solid-state structure of $[\text{Pu}(\text{OH}_2)_9][\text{CF}_3\text{SO}_3]_3$ [45] and the chemical similarity between lanthanide(III) and actinide(III) ions provides strong indications of nine-coordination for the larger ions, but one has probably the same small difference in free energy between eight- and nine-coordination as noted among the lanthanides [46]. Evidence for nine-coordination of $\text{Cm}^{3+}(\text{aq})$ has been obtained from measurements of the fluorescence lifetime [47,48].

4.1.2. Actinide(IV) ions

Johansson et al. [49,50] have studied the structure of $\text{Th}^{4+}(\text{aq})$ and $\text{U}^{4+}(\text{aq})$ in aqueous solution using large angle X-ray scattering and Moll et al. [51] using extended X-ray absorption spectroscopy. As noted above, there are important methodological differences between the two methods, but both give the same metal–water distance within the experimental errors. The LAXS data indicate eight-coordination and the EXAFS data a coordination number of 10 ± 1 . Ankudinov et al. [41] have studied the $\text{Pu}^{4+}(\text{aq})$ ion using XANES and Allen et al. the $\text{Np}^{4+}(\text{aq})$ ion using EXAFS [44]; the $\text{M}^{4+}\text{--OH}_2$ bond distances are consistent with those from Th^{4+} and U^{4+} . Yang et al. [52,53] and Tsushima et al. [54] have provided additional information on the coordination number of Th^{4+} by using quantum chemical methods. Their results indicate that the energy difference between 9- and 10-coordination is very small, about 1 kJ/mol, as compared to about 50 kJ/mol between 8- and 9-coordination [54]. From these data it seems safe to conclude that the coordination number is either 9 or 10, and that equilibrium might exist between the 9- and 10-coordinated ions. The idealized symmetry in 9- and 10-coordination is shown in Fig. 8a and b. The first is a mono-capped and the second a bi-capped square antiprism. The relative energies of U^{4+} and Np^{4+} ions with 8, 9 and 10 coordinated water indicate that the preferred coordination number for U^{4+} is 9, while there might be an equilibrium between 8 and 9 coordination for Np^{4+} [54b].

4.1.3. Actinyl(V) aqua ions

Allen et al. [44] have determined the structure of $\text{NpO}_2^+(\text{aq})$ by using EXAFS and report a composition $\text{NpO}_2(\text{OH}_2)_5^+$ with a pentagonal bi-pyramid geometry with the distances Np--O_{yl} and Np--OH_2 equal to 1.85 and 2.51 Å, respectively. Ankudinov

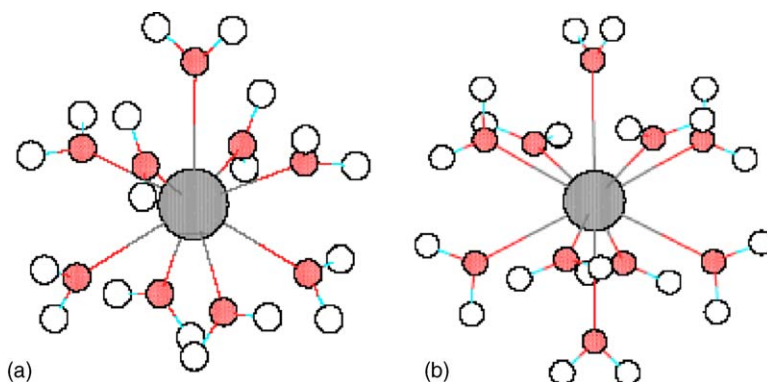


Fig. 8. The structures of: (a) $\text{Th}(\text{OH}_2)_9^{4+}$ in C_{4v} symmetry (mono-capped square antiprism) and (b) $\text{Th}(\text{OH}_2)_{10}^{4+}$ in D_{4d} symmetry (bi-capped square antiprism). The structures are from Yang et al. [52].

et al. [41] and Conradson [55] suggest a similar structure for $\text{PuO}_2^+(\text{aq})$. This geometry is also obtained in a quantum chemical calculation on UO_2^+ by Vallet et al. [56] who suggest a pentagonal bi-pyramid structure very similar to the one found in the uranyl(VI) and neptunyl(VI) aqua ions.

4.1.4. Actinyl(VI) aqua ions

LAXS and EXAFS data from solutions provide bond distances and approximate values of the coordination number. Quantum chemical calculations [56–60] provide a three-dimensional model of these structures, where the bond distances can be compared with experimental LAXS [61,62] and EXAFS [41,44,55] data, e.g. for the uranyl(VI) aqua ion (cf. Table 2 that also contains information on the energy difference between aqua complexes with different coordination numbers), and indicate that all actinyl(VI) ions have the constitution $\text{AnO}_2(\text{OH}_2)_5^{2+}$, despite a suggestion by Neuefiend et al. [62] that there are only four coordinated water ligands, or possibly an equilibrium between four- and five-coordination.

4.2. The constitution and structure of actinide complexes ion solution

The discussion in this section is based on equilibrium analytical data and a combination of spectroscopic, LAXS, EXAFS and quantum chemical information.

4.2.1. Actinide(III) complexes

The constitution of complexes formed in the Cm(III)–glycolate system has been investigated by Stumpf et al. [9] using time-resolved fluorescence spectroscopy. By measuring the fluorescence spectra and the emission lifetime as a function of the glycolate concentration they showed that the glycolate ligand is chelate bonded through the COO^- and OH-groups and that the complex at high glycolate concentration had the composition $[\text{Cm}(\text{HOCH}_2\text{COO})_4(\text{H}_2\text{O})]^-$, complex 1. By increasing the pH in solutions from the range $4.5 < \text{pH} < 6.5$ to higher values they found that the single peak at 602.3 nm was gradually replaced by a second peak at 605.6 nm due to the formation of a new species, complex 2, in rapid equilibrium with complex 1; this complex attains its maximum concentration at pH 9.7 at the same time as the intensity of the first peak decreases. At $\text{pH} > 9.7$, a third peak from a new species, complex 3, appears at 611.3 nm; this complex is in slow equilibrium with the other two. Quantitative analysis of the spectral data indicates that complex 2 is formed from complex 1 by the dissociation of H^+ and complex 3 from complex 2 also by dissociation of H^+ . Complex 2 has the same fluorescence lifetime as complex 1 and its composition might then be either $[\text{Cm}(\text{HOCH}_2\text{COO})_4(\text{OH})]^{2-}$ or $[\text{Cm}(\text{OCH}_2\text{COO})(\text{HOCH}_2\text{COO})_3(\text{OH}_2)]^{2-}$. Slow equilibrium is a typical feature observed when the OH-group in coordinated glycolate is deprotonated (cf. Section 6.3).

Table 2

Experimental bond distances in solution and calculated bond distances for different uranyl(VI) complexes and isomers ((oxalate) denotes a chelate bonded through one carboxylate oxygen donor from each carboxylate group, (oxalate-uni) a ligand coordinated to a single oxygen donor and (ox-carb), an oxalate coordinated using both oxygen donors in the same carboxylate group)

Complex	Bond distances (Å, from EXAFS)	Bond distances (Å, calculated using QM)	Relative energy of isomers (kJ/mol)
$[\text{UO}_2(\text{OH}_2)_5^{2+}](\text{H}_2\text{O})$	U–O _{yl} , 1.77 U–O, 2.41	U–O _{yl} , 1.776 U–O, 2.47	0
$[\text{UO}_2(\text{OH}_2)_4^{2+}](\text{H}_2\text{O})_2$		U–O _{yl} , 1.774 U–O, 2.41	52.9
$[\text{UO}_2(\text{OH}_2)_6^{2+}]$		U–O _{yl} , 1.785 U–O, $4 \times 2.48(1)$ and 2×2.64	11.9
$\text{UO}_2(\text{oxalate})_3^{4-}$	U–O _{yl} , 1.79 U–O _{ox} , 2.37 U–C, 3.30	U–O _{yl} , 1.73 U–O _{ox} , 2.52 U–C, 3.42	37
$\text{UO}_2(\text{oxalate})_2(\text{oxalate-uni})$		U–O _{yl} , 1.73 U–O _{ox} , 2.43 U–O _{ox-uni} , 2.39 U–C, 3.30	0
$\text{UO}_2(\text{oxalate})_2\text{F}^{3-}$	U–O _{yl} , 1.77 U–O _{ox} , 2.44 U–C, 3.31 U–F, 2.22	U–O _{yl} , 1.74 U–O _{ox} , 2.43 U–C, 3.31 U–F, 2.22	0
$\text{UO}_2(\text{oxalate})(\text{ox-carb})\text{F}^{3-}$		U–O _{yl} , 1.73 U–O _{ox} , 2.40 U–C, 3.28 U–O _{carb} , 2.53 U–F, 2.20	9.2

Included are also the relative energies at the MP2 level of different isomers. The QM geometry has been optimized either at the MP2 level in the gas-phase in the case of the uranyl aqua ion or at the SCF level using a PCM solvent model that describes the solvent as a polarizable dielectric continuum with the same dielectric constant as water. The data for the uranyl aquo ion are from [57,79] and for the oxalate complexes from [84].

As the equilibrium between complexes 1 and 2 is fast, the authors suggest that complex 2 has the composition $[\text{Cm}(\text{HOCH}_2\text{COO})_4(\text{OH})]^{2-}$. The fluorescence lifetime of complex 3, 295 μs , is longer than the lifetime for complexes 1 and 2, 206 μs , but still much shorter than in species without coordinated water, 1250 μs . This indicates that complex 3 contains OH-groups from coordinated ligands that transfer the excitation energy. The authors suggest that the stoichiometry is either $[\text{Cm}(\text{OCH}_2\text{COO})(\text{HOCH}_2\text{COO})_3(\text{OH})]^{2-}$ or $[\text{Cm}(\text{OCH}_2\text{COO})_2(\text{HOCH}_2\text{COO})_2(\text{OH}_2)]^{2-}$.

4.2.2. Actinide(IV) complexes

The structure of $\text{ThF}^{3+}(\text{aq})$ has been studied using EXAFS [51] that provides quantitative information on the Th–F and Th–OH₂ bond distances, 2.14 and 2.48 Å, respectively, and a coordination number of approximately 10. Toraiishi et al. [63] studied complex formation in the Th(IV)–glycolate system as a function of pH and deduced an equilibrium model based on potentiometric and NMR data. The potentiometric data indicated the formation of di- and tetra-nuclear complexes and the NMR data provided information on the amount of coordinated oxyacetate, $^-\text{OCH}_2\text{COO}^-$. Preliminary EXAFS data suggested a structure for the tetra-nuclear $\text{Th}_4(\text{OCH}_2\text{COO})_8(\text{OH})_4^{4-}$ complex containing a cubane like “Th₄O₄” core. The corresponding 5-sulfosalicylate system [64] has also been studied in the same way and the data indicate that the complexes formed are very similar to those in the glycolate system.

The limiting carbonate complex of the tetravalent actinides has the composition $\text{An}(\text{CO}_3)_5^{6-}$ [65–67] and the solid-state structure of several compounds that contain isolated $\text{Th}(\text{CO}_3)_5^{6-}$ [68,69] and $\text{Pu}(\text{CO}_3)_5^{6-}$ [67] units are known. There is also EXAFS data from solutions where the complexes $\text{Pu}(\text{CO}_3)_5^{6-}$ and $\text{U}(\text{CO}_3)_5^{6-}$ are predominant [67] and the distances Pu–O and Pu–C are in good agreement with those in the solid state, indicating the same or very similar structures in both phases.

4.2.3. Actinyl(V) complexes

The structure information from solution is limited to EXAFS data for $\text{MO}_2(\text{CO}_3)_3^{5-}$, M = U and Np, $\text{MO}_2(\text{CO}_3)_3^{5-}$, formed at high carbonate concentrations and where the composition has been established by solution chemical methods [70,71]. The complexes are much less stable than the corresponding actinyl(VI) complexes and the mode of coordination of the ligands is therefore not obvious. The structures of $\text{UO}_2(\text{CO}_3)_3^{5-}$ from Docrat et al. [72] and $\text{NpO}_2(\text{CO}_3)_3^{5-}$ from Clark et al. [73] give strong indication that the carbonate ligands are bonded through two oxygen atoms, resulting in a structure very similar to that of $\text{UO}_2(\text{CO}_3)_3^{4-}$; Gagliardi et al. [74] have suggested a detailed structure model by using quantum chemical methods. The agreement between experimental and calculated bond distances in [75] is better than 0.03 Å, a good indicator for the reliability of the model.

4.2.4. Actinyl(VI) complexes

Most experimental structure information has been obtained for uranyl(VI) complexes and we will focus on these data

and begin with a discussion of the number of labile ligands in the equatorial plane. From solid-state structures [75] it is well known that there are compounds with four, five and six equatorial donor atoms, a fact that may result in the formation of structure isomers. The first example is taken from the binary uranyl–fluoride and uranyl–hydroxide systems where the structures of the complexes $\text{UO}_2\text{F}_4(\text{OH}_2)^{2-}$ [76,77] and $\text{UO}_2(\text{OH})_4^{2-}$ [78,79] have been identified in solid state and solution. The uranyl(VI) cation is a very strong Lewis acid and accordingly gives strong complexes with fluoride and hydroxide. The limiting complex has in both cases the composition $\text{UO}_2\text{L}_5^{3-}$, L = OH[−], F[−]; a notable fact is that the equilibrium constant for the reaction $\text{UO}_2\text{L}_4^{2-} + \text{L}^- \rightleftharpoons \text{UO}_2\text{L}_5^{3-}$ is small, 0.4 and 0.6 M^{−1} for the hydroxide and fluoride systems, respectively [80,81]; as a result the $\text{UO}_2\text{L}_4^{2-}$ complexes are predominant over a large range of L concentrations. Hydroxide complexes are in general formed by dissociation of a proton from coordinated water, if this is the case the precursor of $\text{UO}_2(\text{OH})_5^{3-}$ must be $\text{UO}_2(\text{OH})_4(\text{OH}_2)^{2-}$. By combining $K = 0.4 \text{ M}^{-1}$ with the dissociation constant of water, K_W , we notice that the equilibrium constant for the reaction $\text{UO}_2(\text{OH})_4(\text{OH}_2)^{2-} \rightleftharpoons \text{UO}_2(\text{OH})_5^{3-} + \text{H}^+$ is smaller than K_W , i.e. coordinated water would be a weaker acid than the water solvent; this is unlikely in view of the strong inductive effect of uranium on coordinated ligands. The fact that the stepwise equilibrium constant for the formation of $\text{UO}_2\text{L}_5^{3-}$ is very near the same for fluoride and hydroxide indicates that they are formed in the same way, that is by coordination of the ligand from the solution. Solution EXAFS and quantum chemical data provide additional information on the constitution of these complexes. The bond distances for the complex $\text{UO}_2\text{F}_4^{2-}(\text{aq})$ [77] are only consistent with the composition $\text{UO}_2\text{F}_4(\text{OH}_2)^{2-}$, that is the complex contains coordinated water. The EXAFS data from solutions containing $\text{UO}_2(\text{OH})_4^{2-}(\text{aq})$ [78,79] give U–OH bond distances in excellent agreement with those in the solid state; the coordination number is more uncertain and Vallet et al. [77] prefer the composition $\text{UO}_2(\text{OH})_4^{2-}$, that is a complex with no coordinated water, while Clark et al. [78] suggest the composition $\text{UO}_2(\text{OH})_5^{3-}$. Quantum chemical calculations confirm the stoichiometry and structure of $[\text{UO}_2\text{F}_4(\text{OH}_2)^{2-}]$ [77,82] and $[\text{UO}_2(\text{OH})_4^{2-}](\text{H}_2\text{O})$ [77,83]; the water outside the square bracket indicates that it is located in the second coordination sphere.

The relative energy of isomers with different coordination number is particularly important in mechanistic discussions where the identification of intermediates with coordination number different from that of the reactant is essential for mechanistic assignments. These intermediates are usually present in very low concentrations and can therefore not be identified by solution chemical methods.

The ¹⁹F NMR spectrum [10] in Fig. 3 provides an example of the use of NMR methods for the determination of the structure of a complex in solution. There are two peaks with the ratio 1:2 for the complex $\text{UO}_2(\text{acetate})\text{F}_3^{2-}$. The presence of two non-equivalent fluoride ions in the ratio 1:2 is only compatible with a structure where both carboxylate oxygens are coordinated (cf. Fig. 9).

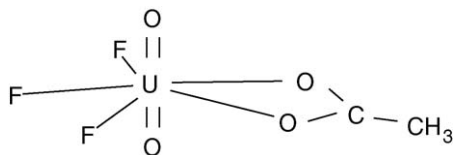


Fig. 9. Coordination geometry of the complex $\text{UO}_2(\text{acetate})\text{F}_3^{2-}$ [10]. The two edge fluorides have the same chemical shift, while the central fluoride is different. This indicates a symmetry plane $\text{F}_{\text{central}}\text{--U--C}$ and coordination of both carboxylate oxygen atoms.

4.2.5. Coordination of multidentate ligands

Equilibrium constants do not provide direct information on the mode of coordination of multidentate ligands, even if the magnitude of the equilibrium constant gives an indication if a chelate is formed, or not; this so-called chelate effect has recently been reviewed [37]. In this section we will discuss the mode of coordination of oxalate and malonate in uranyl(VI) complexes using solution EXAFS data and quantum chemical calculations.

The complex $\text{UO}_2(\text{oxalate})_3^{4-}$ is predominant at high oxalate concentrations where its equilibrium constant has been determined using equilibrium analytical methods (Ref. [84] and those cited there). The magnitude of the equilibrium constant for the reaction $\text{UO}_2(\text{oxalate})_2(\text{OH}_2)^{2-} + \text{oxalate}^{2-} \rightleftharpoons \text{UO}_2(\text{oxalate})_3^{4-}$ is not sufficiently large to indicate if the third ligand forms a chelate, or not. A combination of EXAFS data and quantum chemical structure data suggests that the experimental bond distances are in much better agreement with a model where the third ligand coordinates to one carboxylate oxygen, than a model where it forms a chelate. This conclusion is supported by the relative energy of the two isomers, where the tris-chelated model is 37 kJ/mol less stable than the other one. The situation is less clear for the two isomers $\text{UO}_2(\text{oxalate})_2\text{F}^{3-}$ and $\text{UO}_2(\text{oxalate})(\text{ox-carb})\text{F}^{3-}$, where ox-carb denotes an oxalate coordinated to both oxygen atoms from one carboxylate group. The experimental bond distances are in slightly better agreement with the model with two chelate bonded oxalate ligands; this is also the most stable of the two isomers.

Vázquez et al. [85] have discussed the mode of coordination of the malonate ligand in uranyl complexes based on quantum chemical calculations and EXAFS data. Both methods indicate the formation of a binuclear complex $(\text{UO}_2)_2(\text{malonate})_2(\text{OH})_2^{2-}$ with two hydroxide ions bridging the uranium atoms and with the malonate chelate bonded through one oxygen from each carboxylate group.²

² Geometry optimization of actinide complexes does not always have smooth convergence behavior (in particular for isomers where a ligand with several donor groups is coordinated to only one of them); this is probably a result of several configurations with approximately the same energy. Whenever possible, the geometry optimization should begin in gas phase and then using this optimized structure as a starting point for the geometry optimization in the solvent. Non-electrostatic contributions to the solvation energy and energy gradients, that is dispersion, cavitations and repulsion contributions, should be omitted in the geometry optimization [86].

5. The rate and mechanism of ligand substitution reactions

“Mechanism” is defined as the sequence of elementary reactions that transform the reactant(s) to product(s). The different steps can rarely be studied in isolation, but have to be inferred from the experimental rate equation and the activation enthalpy, entropy and volume, ΔH^\ddagger , ΔS^\ddagger and ΔV^\ddagger , respectively; in addition, the structure and coordination geometry of reactants, intermediates and products give important clues on the microscopic details of the reaction. The rate equation rarely provides a unique mechanistic model because it contains only stoichiometric information on the rate-determining step and the fast equilibria that precedes this and no information on the following elementary reactions.

Most information on rates and mechanisms of ligand substitution reactions in actinide complexes refers to uranium systems, but this in general only includes information on rate equations, while the mechanistic discussions are much more speculative. Lincoln [87] and Tomiyasu and Fukutomi [88] have reviewed reactions in uranyl(VI) systems in non-aqueous solvents, while Nash and Sullivan [89] have reviewed the kinetics and mechanism of actinide redox and complexation reactions in aqueous solution. Vallet et al. [40] have discussed the combination of experimental and quantum chemical methods for the elucidation of the intimate mechanism of solvent exchange and ligand substitution in uranyl(VI) complexes.

Substitution reactions of simple unidentate ligands are in general very fast and require special experimental methods (temperature jump, and other relaxation methods; stopped-flow; NMR spectroscopy). Only the uranyl(VI) fluoride system has been studied in detail [90].

Most of the experimental studies of ligand substitution have been made using multidentate ligands. These reactions involve several elementary reactions such as chelate ring opening/ring closure and ligand dissociation/association steps. In addition, the ligands are often protolytes and the rate equation therefore depends on the hydrogen ion concentration. Ligand substitution reactions with multidentate ligands are conveniently followed using conventional stopped-flow methods. Experiments of this type start from a system that is not in equilibrium and its evolution is then followed until equilibrium has been attained. In many cases the reaction has to be followed by using an indicator and this introduces additional complications when deducing the reaction mechanism (cf. Friese et al. [91]).

A more direct method to obtain mechanistic information on ligand exchange reactions is to use NMR equilibrium dynamics with ^1H , ^{13}C , ^{17}O , ^{15}N and ^{31}P as the NMR-active nuclei. ^{17}O enriched UO_2^{2+} and ternary complexes containing fluoride have been particularly useful as the high sensitivity and wide chemical shift scales of these nuclei make it possible to study a very large range of exchange rates. An example is the exchange reaction $\text{UO}_2(\text{H}_2\text{O})_5^{2+} + \text{H}_2\text{O}^* \rightleftharpoons \text{UO}_2(\text{H}_2\text{O}^*)_5^{2+} + \text{H}_2\text{O}$, that was studied using proton NMR in mixed water–acetone media by Ikeda et al. [92] and Bardin et al. [93] and by ^{17}O NMR in water by Farkas et al. [94]. An analogous example is the exchange between dimethyl sulfoxide (DMSO)

and $\text{UO}_2(\text{DMSO})_5^{2+}$ in DMSO solvent that was studied by Ikeda et al. [95].

It should be noted that NMR spectroscopy is one of the most powerful tools to study ligand exchange reactions at equilibrium. NMR gives information on all reactions that contribute to the dynamics at the reaction centre and one NMR active ligand can then provide information on the dynamics of other ligands that are not NMR active. An example discussed in Section 5.6 is the use of ^{19}F NMR to estimate of the rate of water exchange in $\text{UO}_2(\text{oxalate})\text{F}(\text{H}_2\text{O})_2^-$ and $\text{UO}_2(\text{oxalate})\text{F}_2(\text{H}_2\text{O})_2^{2-}$ [36].

Different experimental techniques can be applied depending on the system and the rate of exchange (that can vary between 10^{-2} and 10^6 s^{-1}); when applied on the same exchange system, these techniques often give complementary information. In systems where the exchange reactions are slow on the time scale determined by their chemical shift difference (T_1 -scale) individual peaks can be observed for the exchanging sites. If the line shape of the signals is not affected by the exchange (T_2 -scale) the kinetic information can be obtained by using one- or two-dimensional (EXSY) magnetization transfer experiments. In the intermediate case, where the exchange rate is still slow on chemical shift scale, but fast enough to affect the line shape of the signals, the rate can be calculated from the line broadening caused by the exchange reaction(s). When the exchange is fast on the chemical shift time scale the rate constants must then be calculated by using the more complex matrix formalism [90].

The NMR active nuclei may be located in different chemical surroundings in the same complex allowing studies of intramolecular exchange, or located in different species, e.g. the complex and the free ligand, making studies of intermolecular exchange possible.

It is often difficult or impossible to use the NMR method to study the rate and mechanism of the formation of the first complex in systems where strong complexes are formed because the free ligand concentration is here very small. In these cases stopped-flow technique is a useful alternative; on the other hand, NMR spectroscopy is superior when studying the rate and mechanism in limiting complexes [36,96].

At best, the experimental methods used in the analysis of reaction mechanisms provide a chemical consistent mechanism for the overall reaction, the so-called stoichiometric mechanism. This is only a first step in the understanding of how the chemical reactions occur, that is the timing of bond breaking and bond formation and the structure of the activated complex. The experimental activation parameters provide indicators for the intimate mechanism; however, they need to be related to a microscopic model in order to provide a firmer basis for mechanistic assignments. Information of this type may be provided by ab initio quantum chemical methods (QM) that provide information on the geometry and relative electronic energy of reactants, the activated complex and intermediates at 0 K and molecular mechanics (MM) and classical trajectory methods from ab initio theory (QM/MM). In order to have information on reactions in solution at ambient temperatures from ab initio methods, it is necessary to use a proper solvent model and to calculate heat capacities of reactants and activated complexes using the molecular partition functions (vibration and rotation) (cf. Section 5.9).

It is not straightforward to calculate the vibration and rotation energy levels; however, QM calculations reveal that the structure of intermediates is often close to that of the activated complex and one can then use the partition functions and the thermodynamic data for the intermediate as a first approximation for those of the activated complex (cf. Section 5.9). When the partition functions are not known it is often assumed that the electronic activation energy is close to the activation enthalpy [40]. Calculations of the activation volume can be made from the geometry of reactants and activated complexes and are therefore very useful for the assignment of mechanisms; however, the calculated volume rests on assumptions inherent in the solvent model used.

Intermediates play an important role in mechanistic discussions; however, they are in general very reactive and can rarely been identified experimentally. The experimental activation enthalpy refers to an ensemble average and the ab initio data to a single “trajectory”; nevertheless, they might be compared in systems where the ligands are strongly bonded. The MM model refers to an ensemble of reactant and solvent molecules that move in a potential field generated by interactions between them, all of which are described by empirical potential functions that include Coulomb interaction and dispersion terms (Lennard–Jones potentials) and repulsion contributions. Inclusion of many-body, polarization and charge transfer effects into these potentials has been investigated by Clavaguéra et al. [97]. So far, very few molecular mechanics or time-dependent MM, usually referred to as molecular dynamics (MD), simulations have been performed on solvated actinide ions. Some aqueous MD simulations using this energy representation have already been performed in order to model differences in Gibbs energy of reaction for uranyl(VI) complexes with various ligands in water solutions [98] or to study solvation of uranyl(VI) in ionic liquids [99]. Yang et al. [52] used the same type of interaction potentials to investigate the structure and dynamics of Th^{4+} aqua ion. Den Auwer et al. [100] have used MD simulations to obtain structure models of uranyl(VI) and neptunyl(VI) aqua ions and of $[\text{NpO}_2(\text{OH})_4]^{2-}$ to simulate their core excitation spectrum with experimental XANES spectra. Molecular dynamics simulations yield information on the structures of hydrated complexes, on the thermodynamics of the reactions studied and on dynamics for systems with reactions that have half-lives in the pico- to nano-second range. This is the time scale for the water exchange between the second coordination sphere of $\text{Th}^{4+}(\text{aq})$ and the bulk solvent [53]. However, ligand substitution and intra-molecular reactions in actinide complexes are much slower (with time scales in the milli- to micro-second range for uranyl complexes) and cannot be studied by molecular dynamics. Structure data can be derived from instantaneous snapshots taken at regular time intervals during the MD simulations [100]. Observed reaction rates are macroscopic averages over a large number of “chemically identical systems” passing with different initial velocities from the reactant valley to the product valley along various trajectories. Thus, to determine the rates, one must either study a large number of trajectories in an approach based on dynamics or introduce statistical theories based on ensemble distributions. Ziegler and Autschbach have discussed dynamic approaches as well as statistical theories in two recent reviews [101a,b].

Most of the examples discussed in the present review deal with the chemistry of actinyl(VI) ions, but some comments will also be made on the chemistry in other oxidation states. The chemical properties of the aquo ions are a natural starting point for discussions of ligand substitution reactions and intramolecular re-arrangements in the coordination sphere. Experimental and QM studies discussed in Section 4.1 show that the actinyl(V) and (VI) ions have the stoichiometry $\text{MO}_2(\text{OH}_2)_5^+$ and $\text{MO}_2(\text{OH}_2)_5^{2+}$ and very similar geometries. The oxygen atoms in the actinyl unit, “ MO_2 ”, are substitution inert under most conditions, while the water ligands are labile and located in, or close to, the plane through M and perpendicular to the MO_2 -axis. Stable linear “ MO_2 ” aqua ions are only formed for the elements U, Np, Pu and Am in oxidation states 5 and 6. This is due to the participation of f-electrons in the $\text{M}-\text{O}_{\text{yl}}$ bonds that are part of the valence shell in the pre-actinoid elements; their absence in the elements after americium is due to the “shrinking” of the f-orbitals into the core. These facts result in a chemistry that is very different from the main-group and d-transition elements, but also from the 4f-elements.

The actinides are “hard” acids using the Pearson terminology and form strong complexes with hard Lewis bases, many of which are also strong Brønsted bases and one must therefore in all ligand substitution reactions consider not only the competition between the different Lewis acids (metal ion and proton), but also proton catalysis.

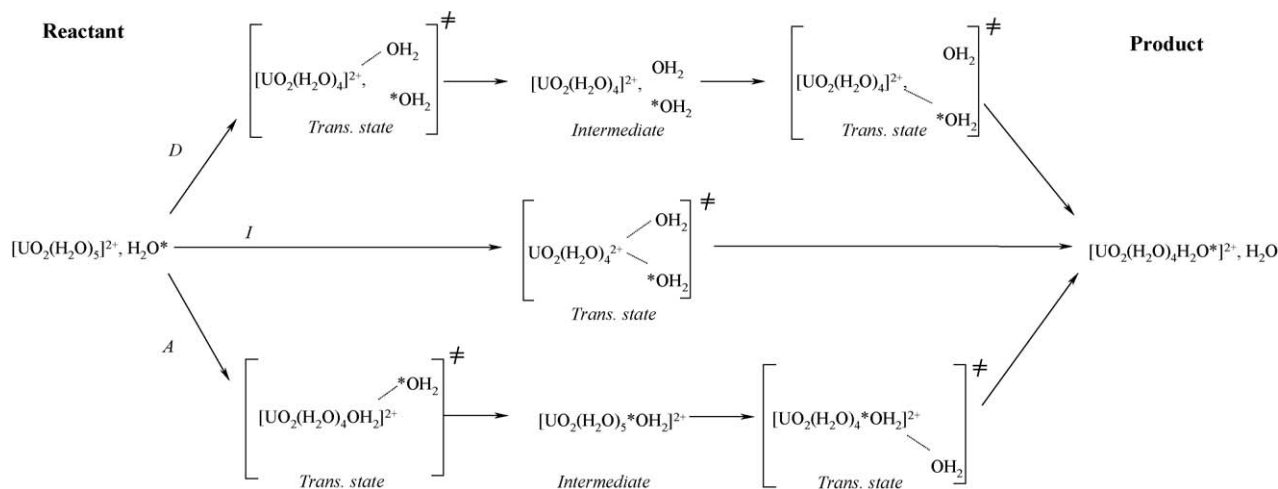
Fluoride and hydroxide are the only simple ligands that form strong complexes with actinides; strong complexes are also formed with ligands with oxygen donors (sulfate, carbonate, phosphate and organic ligands with $-\text{COO}^-$ and $\text{OH}-$ functional groups) and nitrogen donors (organic ligands with aliphatic and aromatic nitrogen donors). The number of donor atoms that can bind to the metal ion in a certain ligand depends on geometrical constraints imposed both by the geometry of the ligand and the preferred coordination geometry of the metal ion; geometrical constraints are therefore important both for the thermodynamic stability of complexes and their reaction mechanisms.

Ligand substitution reactions are categorized as dissociative, D, associative, A, or interchange, I, depending on if intermediates can be identified or not. The D-mechanism is characterized by an intermediate with a lower coordination number than the reactant and the A-mechanism by an intermediate with a higher coordination number. Reactions where no intermediates can be identified are classified as I. The relative energy of the geometry in the ground state and in the intermediates is very important for the mechanistic discussion.

5.1. Mechanisms for water exchange in actinyl(V) and (VI) ions

The rates and the activation parameters for the water exchange in actinyl(VI) aquo ions have been measured experimentally using ^1H and ^{17}O NMR spectroscopy [92–94]. Because of the high rate, the proton NMR data had to be obtained at very low temperature that required the use of a mixed water–acetone medium [92,93]; the ^{17}O data were obtained using a water solvent in the temperature range from -5 to 60°C [94]. There are no experimental determinations of the rate of water exchange in actinyl(V) ions. Quantum chemical calculations using a continuum model (PCM) for the solvent show that the D-intermediate $[\text{MO}_2(\text{OH}_2)_4^{2+}](\text{H}_2\text{O})_2$ has a much higher energy than the A-intermediate, $[\text{MO}_2(\text{OH}_2)_6^{2+}]$, and the ground state $[\text{MO}_2(\text{OH}_2)_5^{2+}](\text{H}_2\text{O})$ for all actinyl(VI) aquo ions [56]. The activation energy for the D-mechanism is also much higher than for the A- and I-mechanisms, both of which have nearly the same value. The calculated electronic activation energy for U(VI) has an estimated uncertainty of about 10 kJ/mol and is in fair agreement with the experimental value. Scheme 3 illustrates the different reaction pathways for the actinyl(VI) aquo ions.

The reaction mechanism for the uranyl(V) aquo ion can only be studied using quantum chemical methods; in this case there is no stable A-intermediate and therefore the exchange most likely follows a dissociative pathway (Table 3). The energy difference between the ground state $[\text{UO}_2(\text{OH}_2)_5^+](\text{H}_2\text{O})$ and the



Scheme 3. The possible reaction pathways for the exchange between coordinated water in $\text{UO}_2(\text{OH}_2)_5^{2+}$ and solvent water as modeled by QM [57]. The scheme shows schematic representations of the reactant, intermediates and transition states in the dissociative (D), associative (A) and interchange (I) pathways. The water in the second coordination sphere is located outside the square bracket.

Table 3

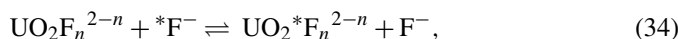
The electronic activation energy, ΔE^\ddagger , and the electronic energy, ΔE_1 , of the D- and A-intermediates relative to the precursor for the water exchange in $\text{MO}_2(\text{OH}_2)_5^{2+}$, M=U, Np, Am and $\text{UO}_2(\text{OH}_2)_5^+$ from Vallet et al. [56]

Complex	D		A		I
	ΔE^\ddagger (kJ/mol)	ΔE_1 (kJ/mol)	ΔE^\ddagger (kJ/mol)	ΔE_1 (kJ/mol)	
$\text{UO}_2(\text{OH}_2)_5^{2+}$	74.0	61.8	18.7	15.8	21.2
$\text{UO}_2(\text{OH}_2)_5^+$	36.4	27.0	–	–	–
$\text{NpO}_2(\text{OH}_2)_5^{2+}$	70.0	68.3	30.0	28.5	–
$\text{AmO}_2(\text{OH}_2)_5^{2+}$	–	67.7	–	22.6	–

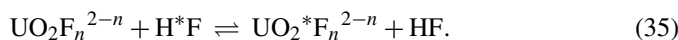
intermediate $[\text{UO}_2(\text{OH}_2)_4^+](\text{H}_2\text{O})_2$ is 27 kJ/mol as compared to 62 kJ/mol for the corresponding uranyl(VI) complexes; the corresponding activation energies are 36 and 74 kJ/mol. The lower activation energy for the D-pathway and the instability of $\text{UO}_2(\text{OH}_2)_6^+$ are presumably a result of a weaker $\text{U}^{\text{V}}\text{--OH}_2$ bonding. We can speculate on the rate constant for the exchange of free and coordinated water in $\text{UO}_2(\text{OH}_2)_5^+$. The reaction is dissociative and one therefore expects positive activation entropy. Hence, the Gibbs energy of activation (and the rate constant) for the uranyl(V) and (VI) ions may not be too different, indicating a rate constant of the order of magnitude 10^6 s^{-1} .

5.2. Mechanisms for fluoride exchange in $\text{UO}_2\text{F}_n^{2-n}$ complexes

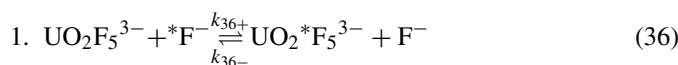
The rate and mechanism of ligand exchange reactions in the binary uranyl(VI)–fluoride system has been studied by Szabó et al. [90]. The complexes formed are strong and the free ligand concentration in equilibrium with the different complexes is therefore small, at least in the concentration range where the complexes UO_2F^+ and $\text{UO}_2\text{F}_2(\text{aq})$ are predominant. In equilibrium systems it is therefore only possible to study the reactions



for $n \geq 3$, while exchange reactions involving HF can be studied for all complexes.



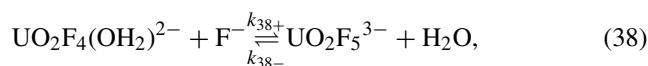
The fluoride ion is small and large steric interference in the different exchange reactions is therefore not expected. Hence, this system is a suitable starting point for a mechanistic discussion before proceeding to ligand substitution reactions in ternary fluoride complexes that also contain large multidentate ligands. The fluoride ion is a moderately strong base and the substitution reactions are therefore proton catalyzed. From the experimental rate equations it is not possible to decide on the role of the solvent in the reactions studied; this is a serious drawback when deducing reaction mechanisms as will be apparent in the following. We will discuss the experimental data for the following exchange reactions:



that follows the rate equation

$$v = k_{\text{obs}}[\text{UO}_2\text{F}_5]. \quad (37)$$

2. Exchange between $\text{UO}_2\text{F}_n^{2-n}$, $n=3-5$, and free fluoride, exemplified by the reaction



that follows the rate equation

$$v = k_{\text{obs}}[\text{UO}_2\text{F}_n^{2-n}][\text{F}^-]. \quad (39)$$

3. At low concentration of fluoride there is exchange between the different complexes $\text{UO}_2\text{F}_n^{2-n}$, as exemplified by



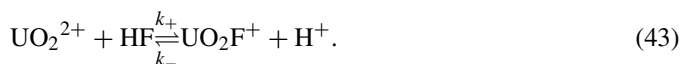
the rate equation is given by Eq. (41) and a similar expression for other complexes:

$$v = k_{\text{obs}}[\text{UO}_2\text{F}_3^-][\text{UO}_2\text{F}_4^{2-}]. \quad (41)$$

4. The fluoride ion is protonated at low pH, making it possible to study exchange reactions:



As an example we will discuss the reaction



The stoichiometric mechanism of the different exchange reactions is deduced from the rate equation and the activation parameters [90]; in addition, QM methods have been used to obtain information at the microscopic level [80].

The equilibrium constant, K_5 , for the reaction (38) is equal to $0.60 \pm 0.05 \text{ M}^{-1}$ [80] and will be used to discuss the fluoride exchange for the reaction (36).

The line broadening of $\text{UO}_2\text{F}_5^{3-}$ in Eq. (36) is independent of the concentration free F^- , indicating a dissociative mechanism with the rate constant $k_{36+} = 6.5 \times 10^3 \text{ s}^{-1}$ at -50°C . Vallet et al. [80] have shown that the line width of the free fluoride signal in the test solutions used to study reaction (36) is a linear function of the concentration of $\text{UO}_2\text{F}_4(\text{OH}_2)^{2-}$ and the rate constant for this pathway is $k_{38+} = 3.65 \times 10^3 \text{ M}^{-1} \text{ s}^{-1}$. The ratio k_{38+}/k_{36+} is equal to 0.56 M^{-1} , very close to the equilibrium constant for reaction (38), indicating this is an elementary reaction and that the exchange (36) is water assisted; additional details are given in [80].

The exchange of fluoride between different complexes is exemplified by reaction (40) with the rate equation (41).

The rate equation is consistent with the fast formation of an outer sphere complex $[\text{UO}_2\text{F}_3^-] \cdots [\text{UO}_2\text{F}_4^{2-}]$ followed by fluoride exchange. Szabó et al. [90] have analyzed these reactions using the Eigen–Wilkins mechanism that describes the stoichiometric mechanism for many ligand substitution reactions. Based on the observation that k_{obs} was of the same order of magnitude as the rate constant for water exchange in $\text{UO}_2(\text{OH}_2)_5^{2+}$, Szabó et al. suggested that the rate-determining step in the fluoride exchange reactions [90] was the dissociation of water from one of the reactants, followed by fast fluoride transfer through a bridge linking the two complexes. It has not been possible to identify a fluoride-bridged intermediate experimentally, but Macak [102] has explored this by using QM methods on the simplest of these exchange reactions:

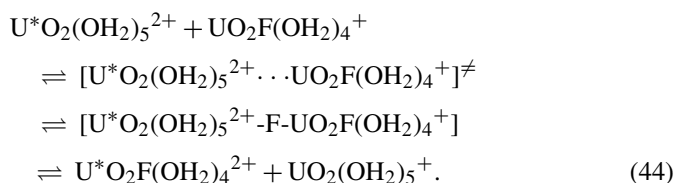


Fig. 10 obtained from this study illustrates how quantum chemical methods can be used to explore mechanistic pathways. Fig. 10a shows the precursor complex $[\text{UO}_2(\text{OH}_2)_5^{2+}][\text{UO}_2\text{F}(\text{OH}_2)_4^+]$, and the associative intermediate in the exchange reaction (44) (Fig. 10b). The U–U distance changes from 6.60 Å in the precursor to 4.62 Å in the intermediate.

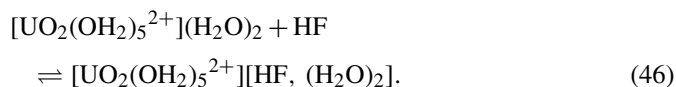
The dissociation of fluoride in ternary complexes is in general slow (cf. Table 4) and it is therefore less likely that the fast exchange reactions in the binary fluoride systems is the result of simple fluoride dissociation from $\text{UO}_2\text{F}(\text{OH}_2)_4^+$.

The simplest exchange reaction involving HF is

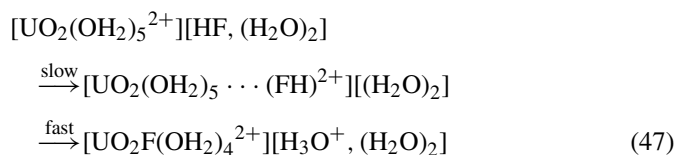


that has been studied both experimentally [90] and using QM methods [103]. The rate constant at 25 °C is $k_+ = 3.2 \times 10^5 \text{ M}^{-1} \text{ s}^{-1}$ and the activation enthalpy 38 kJ/mol; the rate constant is larger in D_2O ($5.8 \times 10^5 \text{ M}^{-1} \text{ s}^{-1}$). Both the rate constant and the activation energy are compatible with a mechanism where U–OH₂ bond breaking is important. The reverse kinetic isotope effect indicates that the formation/dissociation of H–F is important either in the precursor or in the activated complex. This suggestion has been explored in

a QM study of reaction (45) using the following model [103], where $[\text{HF}, (\text{H}_2\text{O})_2]$ denotes the second coordination sphere



A rapid equilibrium reaction leads to the formation of an outer sphere complex that is followed by a rate-determining step where HF enters the first coordination sphere and then transfers a proton to water in the second coordination sphere



This mechanism is consistent with the observed reverse isotope effect as the equilibrium constant for the outer sphere equilibrium in reaction (46) is larger in D_2O than in H_2O as a result of stronger hydrogen bonding.

5.3. Mechanisms for fluoride exchange in ternary uranyl(VI) complexes

Fluoride exchange using ^{19}F NMR line broadening has been studied in a number of different ternary complexes with the composition $\text{UO}_2(\text{X} \cap \text{Y})\text{F}_3$ and $\text{UO}_2(\text{X} \cap \text{Y})_2\text{F}$ that in addition to fluoride contain bidentate ligands, $\text{X} \cap \text{Y}$, like carbonate, acetate, oxalate, glycolate, α -hydroxyisobutyrate, different substituted pyridine-5-carboxylates and glycine. Some data have also been obtained with the multidentate ligand glyphosate. Most of these reactions can be described by the following mechanistic schemes that involve parallel pathways for the F^- and $\text{X} \cap \text{Y}$ exchange reactions (cf. Table 4).

The rate of fluoride exchange in $\text{UO}_2(\text{CO}_3)_3\text{F}_3^{3-}$ is independent on the free carbonate concentration, which is a clear experimental evidence for two parallel pathways. Schemes 4 and 5 show the possible pathways for the exchange of fluoride and bidentate ligands $\text{X} \cap \text{Y}$, in $\text{UO}_2(\text{X} \cap \text{Y})\text{F}_3$ and $\text{UO}_2(\text{X} \cap \text{Y})_2\text{F}$ (charges omitted). Scheme 5 shows that the intermolecular exchange of $\text{X} \cap \text{Y}$ involves a chelate ring opening that is followed by the dissociation of the ligand, where both steps can be water assisted. In general, it is not possible to decide if water participates or not, but there are exceptions, e.g. reaction (36) and the intermediate “ UO_2F_3^- ” formed by disso-

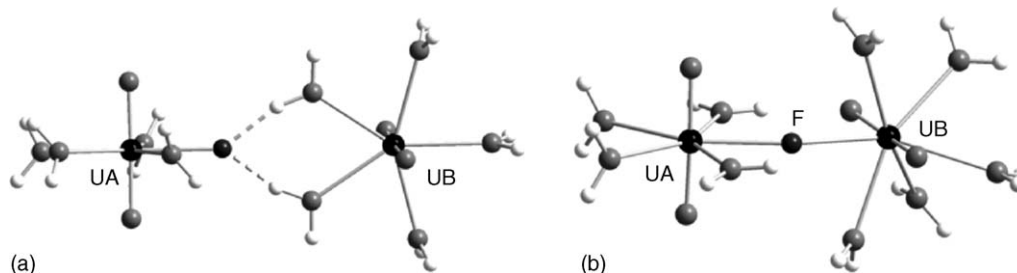


Fig. 10. Structures of the precursor complex $[\text{UO}_2(\text{OH}_2)_5^{2+}][\text{UO}_2\text{F}(\text{OH}_2)_4^+]$ (a) and the intermediate (b) in an associative fluoride exchange reaction $\text{U}^*\text{O}_2(\text{aq})_5^{2+} + \text{UO}_2\text{F}(\text{aq})_4^+ \rightleftharpoons \text{UO}_2(\text{aq})_5^{2+} + \text{U}^*\text{O}_2\text{F}(\text{aq})^+$. The data are from an ongoing study of Macak [102].

Table 4

Rate constants and activation parameters for the intermolecular exchange between free and coordinated $X \cap Y$ and F^- in the binary and ternary uranyl– $X \cap Y$ –fluoride complexes

Complex	Exchanging ligand	Rate constant	Activation parameters		Reference
			ΔH^\ddagger (kJ/mol)	ΔS^\ddagger (J/(K mol))	
$UO_2(\text{acetate})F_3^{2-}$	$\Leftrightarrow ac^-$	$k_+ = 1.3 \times 10^3 s^{-1}$; $k_- = 2.5 \times 10^4 M^{-1} s^{-1}$	–	–	[10]
	$\Leftrightarrow F^-$	$\approx 15 s^{-1}$	–	–	[10]
$UO_2(\text{acetate})_3^-$	$\Leftrightarrow ac^-$	$k_+ = 2.8 \times 10^3 s^{-1}$; $k_- = 3.8 \times 10^5 M^{-1} s^{-1}$	22 (for +)	–61 (for +)	[10]
$UO_2(\text{picolinate})F_3^{2-}$	$\Leftrightarrow pic^-$	$4.7 s^{-1}$	56.2	–16.3	[104]
	$\Leftrightarrow F^-$	24.4^a , $12.8^b s^{-1}$	61.4	14.6	[104]
$UO_2(\text{NO}_2\text{-picolinate})F_3^{2-}$	$\Leftrightarrow N\text{-pic}^-$	$55 s^{-1}$	59.4	11.3	[104]
	$\Leftrightarrow F^-$	$16.0 s^{-1}$	60.3	14.6	[104]
$UO_2(i\text{-pent-picolinate})F_3^{2-}$	$\Leftrightarrow i\text{-pic}^-$	Fast	–	–	[104]
	$\Leftrightarrow F^-$	18.2^a , $13.9^b s^{-1}$	59.7	10.4	[104]
$UO_2(\text{oxalate})F_3^{2-}$	$\Leftrightarrow ox^{2-}$	$6.2 s^{-1}$	70.2	23.1	[104]
	$\Leftrightarrow F^-$	$21.6 s^{-1}$	58.9	12.4	[104]
$UO_2(\text{oxalate})_2F^{3-}$	$\Leftrightarrow ox^{2-}$	$8.7 s^{-1}$	42.9	–73.3	[104]
	$\Leftrightarrow F^-$	$12.3 s^{-1}$	40.8	–74.8	[104]
$UO_2(\text{oxalate})_2^{2-}$	$\Leftrightarrow ox^{2-}$	$1.6 \times 10^3 s^{-1}$	31	–56	[10]
$UO_2(^-OCH_2COO^-)_2^{2-}$	$\Leftrightarrow (HL^-)^c$	$567 M^{-1} s^{-1}$	–	–	[124]
$UO_2(^-OCH_2COO^-)_2F^{3-}$	$\Leftrightarrow (HL^-)^c$	$1.2 s^{-1}$	55.8	–42.1	[124]
	$\Leftrightarrow F^-$	$12 s^{-1}$	45.8	–55.8	[124]
$(UO_2(\text{HO-IBA})F_3^{2-})^d$	$\Leftrightarrow (\text{HO-IBA}^-)^d$	$k_+^d = 250 s^{-1}$; $k_- = 3.1 \times 10^4 M^{-1} s^{-1}$	–	–	
$UO_2(\text{NH}_2\text{CH}_2\text{COO}^-)F_3^{2-}$	$\Leftrightarrow \text{NH}_2\text{CH}_2\text{COO}^-$	$k^e = 2.3 \times 10^{-9} M s$	90	120	[124]
	$\Leftrightarrow F^-$	$48 s^{-1}$	–	–	[124]
$UO_2(\text{CO}_3)F_3^{3-}$	$\Leftrightarrow \text{CO}_3^{2-}$	$5.7 s^{-1}$	–	–	[36]
	$\Leftrightarrow F^-$	$14.2 s^{-1}$	53.7	–15.7	[104]
$UO_2(\text{CO}_3)_3^{4-}$	$\Leftrightarrow \text{CO}_3^{2-}$	$13 s^{-1}$	82	50	[105]
$PuO_2(\text{CO}_3)_3^{4-}$	$\Leftrightarrow \text{CO}_3^{2-}$		34	31	[106]

^a Central fluoride.

^b Edge fluoride.

^c This refers to exchange between coordinated $^-OCH_2COO^-$ and free $\text{HOCH}_2\text{COO}^-$.

^d α -Hydroxy-isobutyric acid.

^e The measured rate constant; this and the activation parameters do not refer to an elementary reaction (cf. Eq. (54) and Scheme 8).

ciation of glycine from $UO_2(\text{NH}_2\text{CH}_2\text{COO})F_3^{2-}$ and CO_3^{2-} from $UO_2(\text{CO}_3)F_3^{3-}$, where “ $UO_2F_3^-$ ” is not identical with $UO_2F_3(\text{OH}_2)^{2-}$ as discussed by Szabó and Grenthe [10,104]. Some other examples based on quantum chemical data will be discussed in Section 5.4.

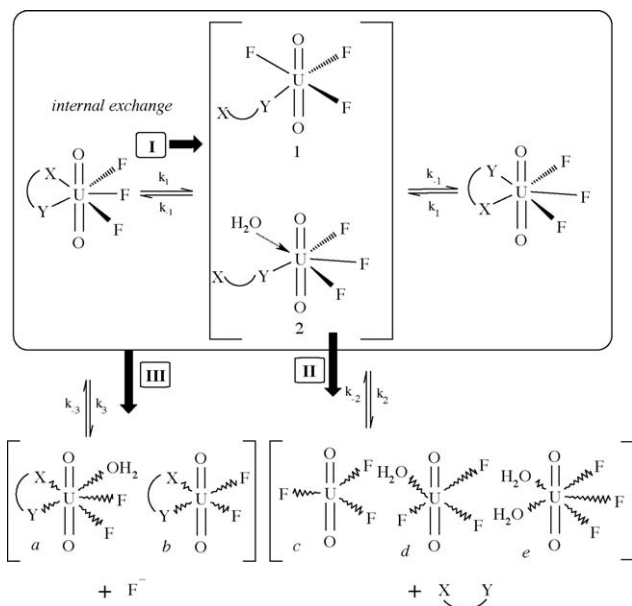
The line broadening of coordinated fluoride depends on *all* dynamic processes in the coordination sphere of uranyl(VI) and can accordingly be used to deduce the dynamics and the reaction mechanisms of these processes. Intra-molecular exchange can only be studied if the chemical surrounding of the coordinated fluoride is different, as in complexes with asymmetric chelating ligands like substituted pyridine-5-carboxylates. Many of these reactions involve the opening/closure of the chelate ring formed by $X \cap Y$.

The rate equation for the exchange between free and coordinated fluoride in these complexes depends only on the concentration of the complex and is independent of the concentration of free ligand, indicating a dissociative mechanism, still with the provision that there is no experimental information on water participation.

5.4. Chelate ring opening/ring closure reactions

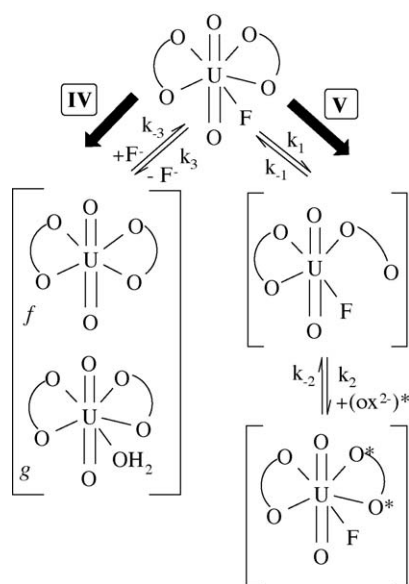
Fig. 11 shows the structure and ^{19}F NMR spectrum of $UO_2(\text{picolinate})F_3^{2-}$, an example of how to use NMR data to obtain information on the rate and mechanism on chelate ring opening/ring closure reactions.

The line broadening indicates a rate of exchange between A and B with the rate constant $300 s^{-1}$, much faster than the exchange between free and coordinated fluoride and picolinate, 13 and $4.7 s^{-1}$, respectively. Hence, the reaction must be inter-molecular. The narrow peak for the central fluoride, which displays spin–spin coupling (a doublet of doublets) between C and the two terminal fluorides, shows no evidence of such fast exchange. This observation is only consistent with a “rotation” of the picolinate ligand that results in exchange of A and B, but not of C; this rotation is the result of chelate ring opening followed by ring closure. The rate constant for the chelate ring opening depends on the stability of the chelate complex and decreases with increasing stability of the complex. This is confirmed by substitutions in the aromatic ring, an electron withdrawing



Scheme 4. The scheme shows the two parallel pathways for dissociation of fluoride and $X \cap Y$ and the consecutive reactions in the exchange between free and coordinated $X \cap Y$ (from Szabó and Grenthe [104], reproduced by the permission of American Chemical Society).

$-\text{NO}_2$ group in the 4-position results in decreased stability of the complex and increased rate constant, $k_{\text{int}} = 2060 \text{ s}^{-1}$ for the intermolecular reaction, while the electron donating 4-(3-pentyl) group in the same position results in a more stable complex and a smaller rate constant, $k_{\text{int}} = 90 \text{ s}^{-1}$, cf. Table 5. This indicates that the chelate ring opening takes place at the N donor. The complex $\text{UO}_2(\text{NH}_2\text{CH}_2\text{COO})\text{F}_3^{2-}$ is an example of a chelate ring opening that is followed by a fast dissociation; this is discussed in Section 6 (Fig. 19 and Scheme 8). The chelate ring opening cannot be studied experimentally in symmetric ligands like



Scheme 5. Parallel pathways for the exchange of oxalate in $\text{UO}_2(\text{oxalate})_2\text{F}_3^{3-}$ with free oxalate (from Szabó and Grenthe [104], reproduced by the permission of American Chemical Society).

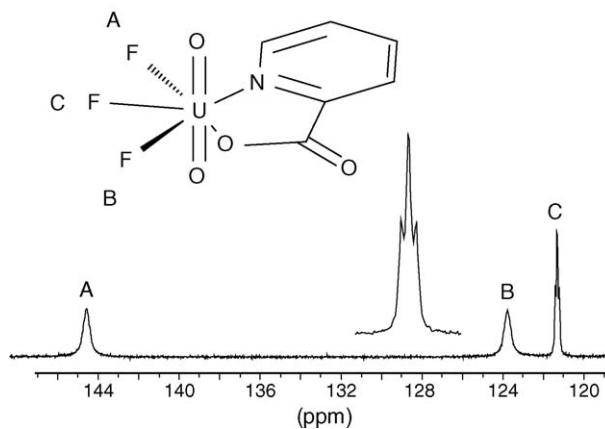


Fig. 11. The ^{19}F NMR spectrum of $\text{UO}_2(\text{picolate})\text{F}_3^{2-}$ at -5°C with peaks for the three different fluorides (from Szabó et al. [36], reproduced by the permission of American Chemical Society). There is no visible spin–spin coupling in the exchanged broadened peaks for fluorides A and B. Spin–spin coupling, a collapsed doublet of doublets, is evident in the narrow peak C.

oxalate; however, quantum chemical methods have been used by Vallet et al. [84] to estimate the electronic activation energy, $\Delta E^\ddagger = 63 \text{ kJ/mol}$ (it was not possible to make the corresponding calculation in the picolate systems, because of computational resources). This value is close to the experimental activation energy for the exchange between free and coordinated oxalate, indicating that the oxalate ring opening is the rate-determining step (cf. Fig. 15).

In the previous sections we have pointed out that experimental data rarely provide information if the reactions studied are water assisted, or not. It is also difficult to use QM methods to decide on this if a reaction is water assisted, or not. The reason is mainly technical; two imaginary modes describing the entering water and the leaving ligand donor have to be identified. As an alternative, the choice of mechanism can be based on the relative energy of the corresponding intermediates, where the preferred mechanism is the one for which the energy of the intermediate is closer to that of the precursor. However, to be confident about the choice, the energy difference between the D- and A-intermediates should not be too small. Vallet et al. [40] have compared the energy of the intermediates $[\text{UO}_2(\text{oxalate-uni})\text{F}_3^{3-}](\text{H}_2\text{O})$ and $[\text{UO}_2(\text{oxalate-uni})\text{F}_3(\text{OH}_2)]^{3-}$ and found that the former is 8 kJ/mol more stable than the latter, indicat-

Table 5

Rate constants and activation parameters for chelate ring opening reactions in uranyl(VI) complexes

Complex	Rate constant (s^{-1})	Activation parameters	
		ΔH^\ddagger (kJ/mol)	ΔS^\ddagger (J/(K mol))
$\text{UO}_2(\text{picolate})\text{F}_3^{2-}$	300	40.1	-46.7
$\text{UO}_2(\text{NO}_2\text{-picolate})\text{F}_3^{2-}$	90	46.8	-32.8
$\text{UO}_2(\text{picolate})_2\text{F}^-$ in CD_3OD	1.44×10^3	26.9	-82.9
$\text{UO}_2(i\text{-pent-picolate})\text{F}_3^{2-}$	2060	49.6	3.3
$\text{UO}_2(\text{NH}_2\text{CH}_2\text{COO}^-)\text{F}_3^{2-}$	129	-	-
$\text{UO}_2(-\text{OCH}_2\text{COO}^-)\text{F}_3^{3-}$	Less than 1.2	-	-

The data refer to -5°C and are reported in [104].

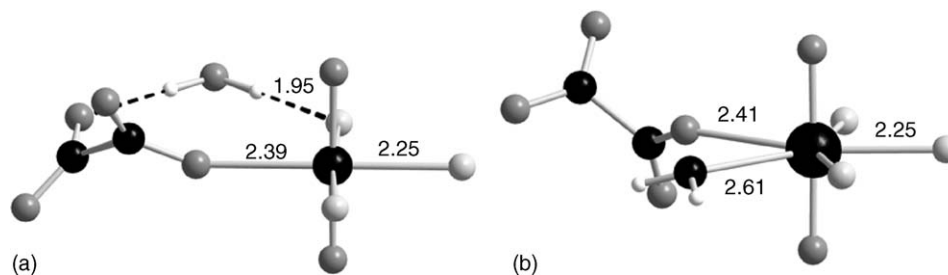


Fig. 12. Perspective view of the: (a) D-intermediate and (b) A-intermediate in the water assisted ring opening reaction in $[\text{UO}_2(\text{oxalate})\text{F}_3^{3-}](\text{H}_2\text{O})$ [40].

ing that the ring opening might take place without assistance of entering water; the two structures are shown in Fig. 12. Another example, the intramolecular exchange of oxalate in $\text{UO}_2(\text{oxalate})_3^{4-}$, will be discussed in the following.

Chelate ring opening/ring closure reactions are important for exchange reactions between structure isomers as exemplified by the $\text{UO}_2(\text{picolate})_2\text{F}^-$ complexes in Fig. 13a. The rate of exchange between them is fast and can only be studied in CD_3OD at low temperature; as the rate of exchange between free and coordinated fluoride is slow the exchange between the different isomers cannot be a result of fluoride dissociation and re-entry at a different site. The situation is different in $\text{UO}_2(\text{acac})_2\text{L}$, where acac is the enolate, $\text{CH}_3\text{C}(\text{O}^-)\text{CH}(\text{O})\text{CH}_3$, of acetylacetone and L an uncharged ligand like dimethylsulfoxide [92]. In this complex ^{13}C NMR data indicate exchange between the non-equivalent methyl groups in the complex that is much faster than the rate of exchange between free and coordinated acetylacetone.

This is the result of dissociation of coordinated L and re-entry opposite its original location, resulting in a change of the chemical surrounding of the methyl groups (Fig. 13b). The high rate, as compared to that in fluoride complexes, is presumably a result of different bonding strength of L and F^- .

As indicated in previous sections, equilibrium thermodynamics gives no information on the presence of isomers in solution; isomers have in some cases been identified using NMR but in cases where this method cannot be used, QM methods may be of assistance. Vallet et al. [84] have studied intra-molecular ligand exchange in the complex $\text{UO}_2(\text{oxalate})_2(\text{oxalate-uni})^{4-}$ with the structure shown in Fig. 14. Possible exchange pathways and intermediates for reactions that are *not* water assisted are shown in Scheme 6.

Mechanism B is the one with the lowest (electronic) activation energy and should therefore be the preferred one. However, the authors have not explored the pathways where the chelate

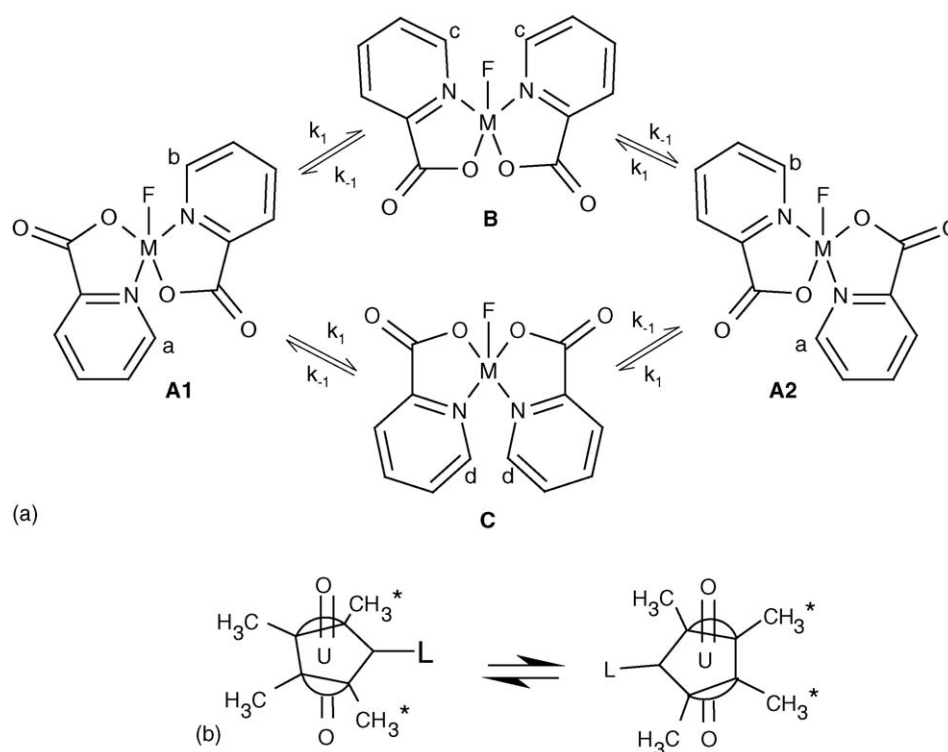


Fig. 13. (a) Structure isomers in the complex $\text{UO}_2(\text{picolate})_2\text{F}^-$ and exchange pathways between them (from Szabó et al. [36], reproduced by the permission of American Chemical Society). (b) Mechanism for the apparent intra-molecular exchange between the two methyl groups in $\text{UO}_2(\text{acac})_2$, where acac denotes acetylacetonate. The exchange takes place by dissociation–re-entry of the ligand L; this is an uncharged ligand like dimethylsulfoxide (DMSO), containing an oxygen donor [96].

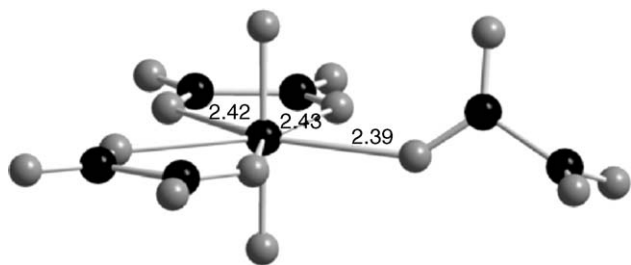


Fig. 14. The most stable structure of the different structure isomers of the complex $\text{UO}_2(\text{oxalate})_3^{4-}$ [84].

ring opening reactions take place with water participation. From the geometry of the complexes it is obvious that mechanism A is the one where water participation may be important and Vallet et al. [40] have therefore compared the relative energy of the intermediates $[\text{UO}_2(\text{oxalate})(\text{oxalate-uni})_2^{4-}](\text{H}_2\text{O})$ and $[\text{UO}_2(\text{oxalate})(\text{OH}_2)(\text{oxalate-uni})_2^{4-}]$, where the latter is 80 kJ/mol more stable than the former; this strongly indicates a much lower activation energy for the water assisted mechanism A, that might even be lower than in the non-water assisted pathway B. There are no experimental data to corroborate these modeling results; the example is intended to demonstrate how QM may be used to assist the experimentalist when suggesting reaction mechanisms.

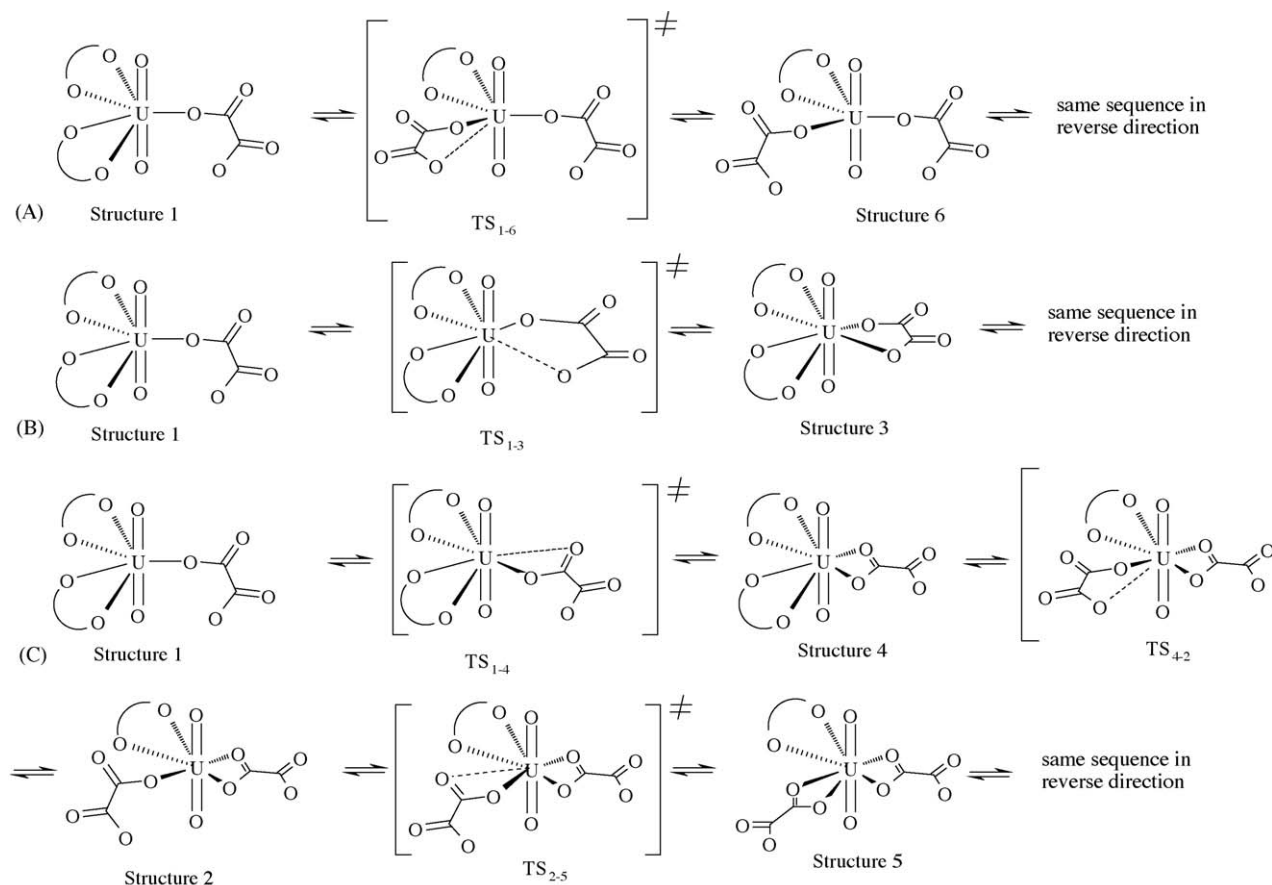
5.5. Inter-molecular exchange between free and coordinated chelate ligands

The experimental data given in Table 4 for different exchange reactions can be discussed using Schemes 4–6; they involve two steps, first a chelate ring opening and then the exchange with free $\text{X} \cap \text{Y}$. We will use Scheme 4 as an example. As no ring-opened intermediate could be identified Szabó and Grenthe [104] used the steady-state approximation to obtain the following rate equation:

$$v = \frac{k_1 k_2}{k_{-1} + k_2} [\text{UO}_2(\text{X} \cap \text{Y})\text{F}_3^{2-}] \cong \frac{k_1 k_2}{k_{-1}} [\text{UO}_2(\text{X} \cap \text{Y})\text{F}_3^{2-}]. \quad (48)$$

For the picolinate system $k_1 = 300 \text{ s}^{-1}$ and $k_1/k_{-1} < 0.05$ (the equilibrium constant for the ring opening), hence $k_{-1} \cong 6 \times 10^3 \text{ s}^{-1}$. The steady-state approximation gives $k_2 \cong 90 \text{ s}^{-1}$, that is $k_{-1} \gg k_1 > k_2$, indicating that the approximation is reasonably good. The activation enthalpy for the picolinate exchange (Tables 4 and 5) is larger than that for the chelate ring opening, indicating the importance of the second step for the overall reaction.

Fig. 15 is a schematic representation of the energy–reaction coordinate diagram for picolinate and oxalate ligand exchange. In the first system the rate-determining step is the dissociation



Scheme 6. Possible mechanisms for the exchange of free and coordinated oxalate in $\text{UO}_2(\text{oxalate})_3^{4-}$. Schematic structures of the various intermediates and transition states are given (from Vallet et al. [84], reproduced by permission of American Chemical Society).

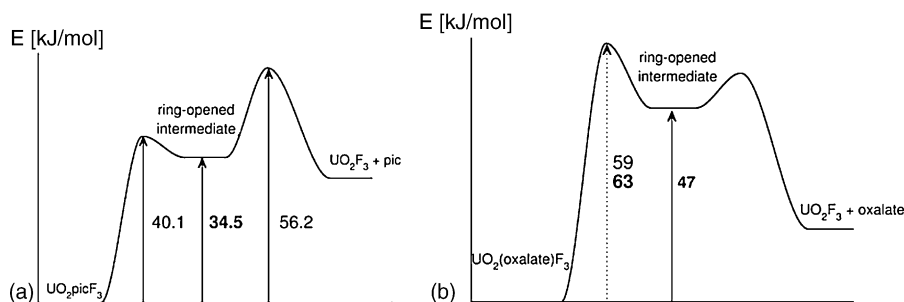
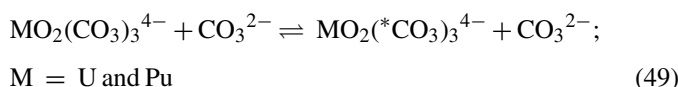


Fig. 15. Potential energy–reaction coordinate diagrams for the intermolecular exchange of: (a) picolinate and (b) oxalate. The activation energies in $\text{UO}_2(\text{picolinate})\text{F}_3^{2-}$ are experimental values and demonstrate that the slow step in the reaction is the dissociation from the ring-opened intermediate. The electronic energy (Vallet et al., unpublished QM results) of the ring-opened intermediate, 34.5 kJ/mol, is close to the value of the activation energy for the chelate ring opening as one expects for an intermediate with so short lifetime that it cannot be identified experimentally. In the $\text{UO}_2(\text{oxalate})\text{F}_3^{3-}$ the experimental activation energy for the total reaction, ring opening and dissociation of oxalate, is 59 kJ/mol. As the calculated activation energy for the chelate ring opening, 63 kJ/mol, is very close to this value, Vallet et al. [40] suggest that the chelate ring opening is the rate-determining step in the intermolecular oxalate exchange.

of the ring-opened intermediate; in the second it is the chelate ring opening as suggested by the fact that the calculated activation energy for the oxalate ring opening, 63 kJ/mol, is close to the experimental value for the exchange between free and coordinated oxalate, 59 kJ/mol. The lifetime of the intermediates is determined by the magnitude of the surrounding activation barriers; these are small, about 5 and 15 kJ/mol in the picolinate and oxalate systems, respectively. The corresponding lifetimes are in the nano-second range [57, Eq. (15)] and can therefore not be identified by the experimental method used.

The ligand exchange for the reaction



has been studied by Brücher et al. [105] and by Clark et al. [106] and both groups conclude that the reactions follow a dissociative mechanism. A strong support for this conclusion is obtained by comparing the activation parameters for reaction (49) with the enthalpy of reaction for (50)



For reaction (49) we have: $\Delta H^\ddagger(\text{U}) = 82$ kJ/mol and $\Delta H^\ddagger(\text{Pu}) = 34$ kJ/mol; for reaction (50) $\Delta H_r(\text{U}) = -57.7$ kJ/mol and $\Delta H_r(\text{Pu}) = -11.6$ kJ/mol. The decrease in activation enthalpy between U and Pu for the exchange reaction is numerically very close to the decrease in the enthalpy of dissociation of carbonate in reaction (50).

The ligand exchange in the ternary acetate system and the glycolate system at low pH presents some additional mechanistic features. The acetate system can be used as a model and we will discuss the reactions using Scheme 7.

The acetate and fluoride exchange in $\text{UO}_2(\text{acetate})\text{F}_3^{2-}$ follows separate pathways as in the other investigated ternary systems; however, the acetate exchange is much faster than the fluoride exchange, while the reverse is the case in the other systems studied. Therefore, the ^{19}F line broadening depends on contributions from both pathways (1) and (2) in Scheme 7.

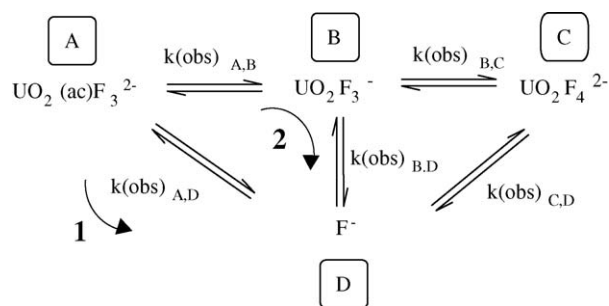
The rate constant for the direct pathway (1) is 15 s^{-1} , in the range of the values found in many other ternary systems; the rate constant for the acetate dissociation is 1300 s^{-1} .

5.6. Water exchange in uranyl(VI) complexes

Direct experimental determinations of the water exchange in uranyl(VI) complexes have only been made for the aquo ion as described previously. An indirect experimental determination has been made using the line broadening of ^{19}F in the complexes $\text{UO}_2(\text{oxalate})\text{F}_2(\text{OH}_2)^{2-}$ (Fig. 6) and $\text{UO}_2(\text{oxalate})\text{F}(\text{OH}_2)_2^-$ (Fig. 16) with the structures given in Figs. 7 and 17.

The line broadening is a result of an intra-molecular fluoride exchange. This is *not* a result of ring opening/ring closure of the oxalate as “rotation” of this symmetric ligand does not result in a site exchange of the fluorides; it is also not a result of dissociation of oxalate or fluoride as these rate constants are much smaller than that for the intra-molecular site exchange, $k_{\text{int}} = 1600 \text{ s}^{-1}$. The only other exchange mechanism that can result in fluoride site exchange is dissociation and re-entry of water; the observed rate constant refers to this reaction. The exchange mechanism is the same between the isomers in $\text{UO}_2(\text{oxalate})\text{F}(\text{OH}_2)_2^-$ and the corresponding rate constant is 1800 s^{-1} . The rate constant is about 250 times slower than the rate of exchange in $\text{UO}_2(\text{OH}_2)_5^{2+}$.

Szabó et al. [90] have discussed the mechanism for the exchange reactions in binary uranyl(VI) fluoride complexes using the Eigen–Wilkins mechanism (cf. Section 5.2), and find that many of the experimental rate constants are consistent with a rate of water exchange slightly above 10^5 s^{-1} ; this is somewhat less than the rate of exchange in $\text{UO}_2(\text{OH}_2)_5^{2+}$,



Scheme 7. Reaction pathways for the exchange of acetate and fluoride in $\text{UO}_2(\text{acetate})\text{F}_3^{2-}$ (from Aas et al. [10], reproduced by the permission of the Royal Society of Chemistry).

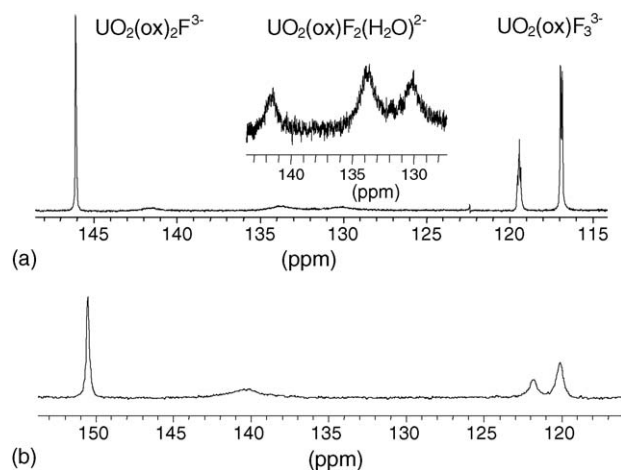
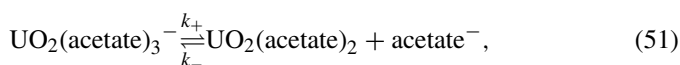
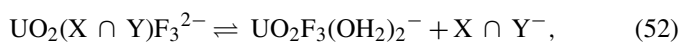


Fig. 16. The NMR spectrum of $\text{UO}_2(\text{oxalate})\text{F}(\text{OH}_2)_2^-$ at: (a) -5°C and (b) 25°C (from Szabó et al. [36], reproduced by the permission of American Chemical Society). The three peaks at 130, 134 and 141.5 ppm correspond to a total of three different fluoride sites in the two isomers in Fig. 17.

$k_{\text{ex}} = 1.3 \times 10^6 \text{ s}^{-1}$. The same mechanism has also been used in a discussion [10] of the acetate exchange in the reaction



where $k_- = (3.8 \pm 0.1) \times 10^5 \text{ M}^{-1} \text{ s}^{-1}$. Using a value of $K_{\text{OS}} = 0.3$, the equilibrium constant for the outer sphere complex in the Eigen–Wilkins mechanism they find a rate constant for the water dissociation equal to $1.3 \times 10^6 \text{ s}^{-1}$ at -5°C , slightly larger than the value for the water exchange in the penta-aquo ion at the same temperature, $4.1 \times 10^5 \text{ s}^{-1}$. Similar results are also obtained for the exchange reaction



where $\text{X} \cap \text{Y}$ is acetate and α -hydroxyisobutyrate. The rate constant for the water exchange based on the Eigen–Wilkins mechanism is here 3.4×10^5 and $4.2 \times 10^5 \text{ s}^{-1}$, respectively. These experimental findings suggest that the uranium–water bond breaking is important in the intimate mechanism.

In view of the large chemical similarity of actinide ions in the same oxidation state, many of the conclusions from the uranyl(VI) data ought to be applicable also for the other actinyl(VI) ions, with the important exception of their redox properties. Frei and Wendt [107] have also used the Eigen–Wilkins mechanism to explain the rate of formation the complexes UO_2NO_3^+ and UO_2SCN^+ .

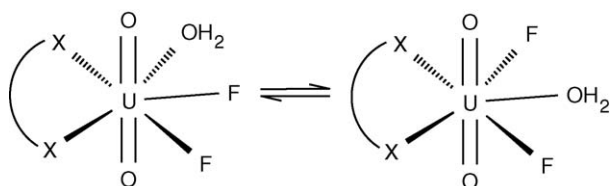


Fig. 17. The two isomers for $\text{UO}_2(\text{oxalate})\text{F}_2(\text{OH}_2)_2^-$ and their exchange mechanism [36].

5.7. Reaction mechanisms in actinyl(V) complexes

Vallet et al. [56] have studied the mechanism for water exchange using QM methods and suggest that it is dissociative, rather than associative/interchange as in actinyl(VI) aquo ions. They relate this to the lower effective charge of the actinyl(V) ion, making the $\text{M}-\text{OH}_2$ bonds weaker. Vallet et al. [56] also noticed that the charge of the actinyl(V) oxygen atoms is more negative than in actinyl(VI) ions, making them stronger Lewis bases. This is consistent with the observations that actinyl(V) ions can form cation–cation complexes with other ions, such as UO_2^{2+} , Cr^{3+} , etc.

The rate and mechanism of exchange between free and coordinated carbonate in $\text{UO}_2(\text{CO}_3)_3^{5-}$ have been studied by Mizouka et al. [108]. The rate equation is $v = k_{\text{obs}}[\text{UO}_2(\text{CO}_3)_3^{5-}]$ with a rate constant $k_{\text{obs}} = 1.13 \times 10^3 \text{ s}^{-1}$ at 25°C and the activation parameters $\Delta H^\ddagger = 62 \text{ kJ/mol}$ and $\Delta S^\ddagger = 22 \text{ J/(K mol)}$. The rate constant is much larger than that in the corresponding uranyl(VI) system ($k_{\text{obs}} = 2.3 \text{ s}^{-1}$) where the mechanism is also dissociative. The activation enthalpy is 20 kJ/mol lower than in the corresponding uranyl(VI) system indicating a weaker bonding of the carbonate ligand. This is consistent with the equilibrium constant for the reaction $\text{UO}_2(\text{CO}_3)_3^{5-} \rightleftharpoons \text{UO}_2(\text{CO}_3)_2^{3-} + \text{CO}_3^{2-}$ that is about three orders of magnitude smaller than for the corresponding uranyl(VI) reaction. These observations provide strong support for the proposed dissociative mechanism [108].

5.8. Reaction mechanisms in actinide(IV) and actinide(III) aquo ions

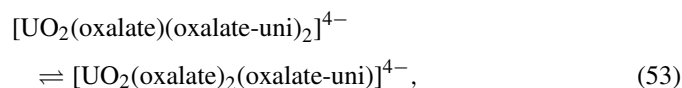
The rate and mechanism of water exchange reactions have been studied for the $\text{U}^{4+}(\text{aq})$, $\text{Th}^{4+}(\text{aq})$ and the $\text{UF}^{3+}(\text{aq})$ ions. The rate constant for the water exchange is $>5 \times 10^7 \text{ s}^{-1}$ for $\text{Th}^{4+}(\text{aq})$ and $5.4 \times 10^6 \text{ s}^{-1}$ for $\text{U}^{4+}(\text{aq})$ and $\text{UF}^{3+}(\text{aq})$; the activation parameters for the two uranium ions are $\Delta H^\ddagger = 34 \pm 3$ and $36 \pm 4 \text{ kJ/mol}$, respectively, and $\Delta S^\ddagger = -16$ and 3 J/(K mol) , respectively; the error in the experimental activation entropy is large, about 15 J/(K mol) . The coordination number of the aquo ion is 10 ± 1 ; eight-coordination can be excluded according to Yang et al. [53]. This suggests that the water exchange is associative or interchange if the coordination number is 9 and dissociative if it is 10 [52]. The computed activation energy for the A and D reaction paths for the Th(IV) system is 15.1 and 12.6 kJ/mol, respectively, are not too far from the experimental value for U^{4+} . It is also of interest to note that the rate constant for the water exchange decreases significantly between Th^{4+} and U^{4+} ; a similar change is observed also in the early part of the lanthanide(III) series.

The chemistry of the actinide(III) is very similar to that of the lanthanide(III) elements.

5.9. Entropy changes in chemical reactions

The experimental activation entropy is often used as a mechanistic indicator; positive activation entropy suggests a D-mechanism, and a negative value an A-mechanism. There are to

our knowledge no accurate theoretical estimates of the activation entropy for reactions in solution. Intermediates for which the surrounding activation barriers are small (as is the case for reactive intermediates) have structures and thermodynamic properties that do not differ much from the corresponding activated complexes and they may therefore be used as approximations for the activated complexes. For this reason Vallet et al. [37] have used QM to determine the entropy of reaction between the precursor and the intermediate to investigate if this can be used as a mechanistic indicator; they find that the entropy change is negative for chelate ring closure reactions such as



that result in an increase in the coordination number. This is an associative reaction for which the standard texts [109] suggest negative activation entropy. Vallet et al. [37] have also used quantum chemical data to discuss the entropy of reaction and especially the so-called “chelate effect”. The large stability of chelate complexes is a result of large positive entropy of reaction. The microscopic “explanation” is that the larger the number of coordinated donor groups, the larger the number of water ligands “released” from the first coordination sphere, a process that has been ascribed to result in a large contribution of the translation entropy. The QM study of Vallet et al. [37] shows that this cannot be the explanation; the translation entropy does not even in gas-phase give the main contribution to the chelate effect and they conclude that there is no simple explanation of the high stability of chelate complexes; it is a result of both enthalpy and entropy contributions that vary from one system to the other.

6. Ligands of biological interests

Metal ions in biological systems are able to coordinate to a variety of biomolecules, e.g. to proteins (especially to the heteroatoms located in their side chains (N, O and S) or to the amide bond), to nucleic acids (in many different ways, to phosphates, to base N-donor atoms or to sugar O-atoms) and to carbohydrates or lipids (C–O and P–O groups) [110,111]. The great variety of coordinating sites in these large molecules makes it difficult to describe the complex formation using “classical” solution chemical methods. In vivo systems are in general not equilibrium systems and the reaction between metal ions and ligands is part of a complex system of equilibria, transport and storage. Duffield et al. have made a short review of some aspects of the biochemistry of actinides [112].

Even though the actinides are not essential elements in living systems, some of them are known to have multiple target organs or tissues in which the specific effect and mode of action depend on interactions with biomolecules [112,113]. The interaction between actinide ions and the surrounding neighbours (ligands) in biological systems may have a large effect on other biological processes, both natural ones and those induced by human activities (e.g. pollution and cleaning). Although there are well-documented examples, the modes of action of actinide ions at the molecular level are still poorly characterized.

The behavior of actinides in the biological systems cannot be separated from their fundamental chemistry; hence, the use of small molecules as model compounds is a widely used approach in the study of these systems. The purpose of these models is not necessarily to duplicate natural properties but to focus on specific questions such as the elucidation of fundamental aspects of structure, bonding and chemical reactivity. There have been relatively few studies on the interaction of actinide ions with ligands in biological systems and of the thermodynamic stability of their complexes. The reason for this is the experimental difficulties due to the radiotoxicity of the transuranium elements. Most of the studies have therefore been made using uranium(VI) and thorium(IV) to predict the chemistry of other actinides with the same oxidation state.

6.1. Amino acids, peptides

We begin the discussion with a short overview of the possible coordination modes of the amino acids and peptides, and then give an example of the ligand exchange dynamics for glycine studied in the uranium(VI)–glycine–fluoride system.

It is well known that amino acids exist in the “zwitter”-ionic form (Fig. 18). Amino acids and peptides possess a number of different functional groups, e.g. carboxyl, hydroxyl and amino (or amido) groups, that can be used for complexation with actinides. In addition, there are amino acids with other functional groups, for example, serine (R: –CH₂–OH) or aspartic acid (–CH₂–COO[–]). All functional groups are both Lewis and Brønsted acids/bases and the mode of coordination is therefore pH dependent; the log *K* values for the protonation equilibria of the amino and carboxyl group are approximately 9 and 2, respectively. Accordingly, potentiometric data show that the protonation of the amino group prevents chelate formation at lower pH (2–4) and the amino acids are then coordinated only via the carboxylate oxygens, in the case of uranium(VI) in a bidentate fashion [114]. At higher pH the amine nitrogen is deprotonated and chelates are formed with N, O coordination. In cysteine (R: –CH₂–SH) the mercapto group is not involved in the complex formation, only the α-amino acid moiety is coordinated, reflecting the “hard” acceptor character of the uranyl ion and the preference of nitrogen over sulfur donors [115]. Similarly, there is no evidence for the coordination of aliphatic hydroxyl group, either in serine (R: –CH₂–OH) or in threonine (R: –CH(CH₃)–OH) [115]. In case of aspartic acid (R: –CH₂–COO[–]), a chelate is formed by the coordination of the carboxylate oxygens instead of the amino group as indicated by ¹³C NMR chemical shift changes of the ligand upon

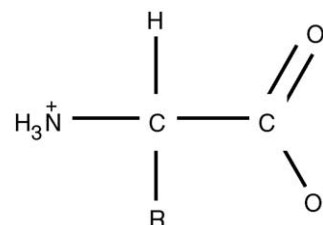


Fig. 18. The “zwitter”-ionic form of amino acids.

coordination with uranium(VI) [116]. On the other hand, the higher stability constant of thorium(IV) complexes with aspartic acid indicates a tridentate coordination via both carboxylates and the amino group [117]. Several factors affect the stability of the complexes, such as the size of the chelate ring, the steric and inductive effects of the substituent at the α -carbon [118–120]. For example, the stability constant for the complex with the six-membered ring formed in the binary uranium(VI)- β -alaninate ($\text{H}_2\text{N}-\text{CH}_2-\text{CH}_2-\text{COO}^-$) system is two orders of magnitude larger than that for the corresponding complex with the five-membered ring with glycine ($\text{R}: -\text{H}$) [121]. Potentiometric and calorimetric studies show that at lower pH only the carboxylate end of a dipeptide (glycylglycine) is coordinated to uranium(VI) [122]; however, the results on the structure of the chelates formed at higher pH are contradictory and it can be questioned if the nitrogen or the oxygen of the peptide group is involved in the ring formation beside the carboxylate end [123]. Huang et al. have recently studied the coordination of uranium(VI) to certain peptides in blood serum [124]. They used various spectroscopic methods (UV-vis, IR, fluorescence and NMR spectroscopy) to study the interaction between peptides and triscarbonato-uranium(VI), $\text{UO}_2(\text{CO}_3)_3^{4-}$, which is the predominant uranium(VI) species in blood serum under physiological conditions. According to their results, one carbonate ligand in this complex can be replaced by a carboxylate group of the studied peptides to form ternary uranium(VI)-carbonate-peptide complexes. The association constants of these peptides to the uranyl bis-carbonate complex are approximately the same as the binding constant of amino acids coordinated by only the carboxylate end to the uranyl ion; infrared spectra confirm this mode of coordination of the peptides. These results indicate a non-specific binding of uranium(VI) to carboxylate group(s) in the presence of carbonate and this model is plausible also for the interactions between the uranyl ion and peptides *in vivo*.

Szabó and Grenthe have studied the ligand exchange dynamics in the ternary uranium(VI)-glycine-fluoride system by NMR spectroscopy [125]. As mentioned before, ^{19}F is an excellent NMR nucleus with very large chemical shift differences between the signals for the coordinated sites in uranium(VI) complexes. Fluoride can very easily replace water molecules in the first coordination sphere, and prevent hydrolysis and the formation of hydrous oxides, which could lead to precipitation at higher pH. At the same time the spectral parameters of the ^{19}F NMR signals (chemical shift, intensity and coupling constants) provide information about the coordination mode of the third ligand in a ternary system, in the present case about the coordination of glycine.

As shown in Fig. 19 (spectrum B), the appearance of three fluorine signals with equal intensities recorded in the ternary uranium(VI)-glycine-fluoride system indicates the formation of one major ternary species and proves unambiguously the bidentate coordination of glycine at pH 8 via the amino group and one of the carboxylate oxygen in a complex with pentagonal bi-pyramidal geometry.

In case of a bidentate carboxylate coordination of glycine one would expect only two fluorine signals with the intensity ratio

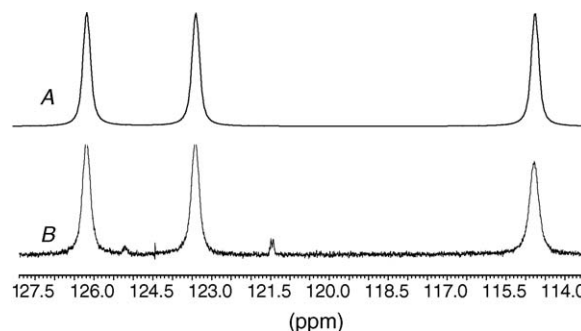


Fig. 19. Measured (B) and calculated (A) ^{19}F NMR spectra (from Szabó and Grenthe [125], reproduced by the permission of American Chemical Society) of the complex $\text{UO}_2(\text{glycine})\text{F}_3^{2-}$ (10 mM UO_2^{2+} , 300 mM glycine and 200 mM fluoride, pH 8.5). The free fluoride signal at around 0 ppm is not shown.

of 1:2 as observed in the corresponding ternary fluoride-acetate uranium(VI) complex discussed in Section 5.5.

The line width of the coordinated fluorides is the same, indicating the same dynamics at each fluoride site. The line shape is affected by both the intermolecular fluoride and glycine exchange reactions. This is important, as ^1H NMR spectroscopy cannot be used in this system to study glycine exchange because the methylene signal of the coordinated glycine coincides with the solvent water signal. Hence, all dynamic information must be based on ^{19}F NMR experiments. The exchange reaction with free fluoride and the internal exchange between the coordinated fluorides was studied by one-dimensional magnetization transfer experiments. The rate constants for the exchange between free and coordinated fluoride and the intra-molecular exchange between the different fluoride sites were obtained by inverting the free fluoride signal (not shown in Fig. 20) and each fluoride signal in the complex. Two pseudo-first-order rate constants for the reactions were obtained from a non-linear fitting of the time dependence of the signal intensities. The rate constant for the exchange between free and coordinated fluoride was 48 s^{-1} ; the second rate constant 70 s^{-1} is the sum of the exchange with both external fluoride and external glycine. The identical line width of the fluorine signals can be explained as follows: if the glycine chelate ring opening is followed immediately by the dissociation of the glycine then the reverse reaction, the coordination of glycine, results in a site exchange between the fluorides without F-U bond breaking. Site exchange between the fluorides due to the internal rotation of the glycine can be excluded as this would result in line broadening of only two fluoride sites as observed in the ternary uranium(VI)-picolinate-fluoride system for the picolinate ligand [36]. The agreement of the line widths in the measured and the calculated spectra (Fig. 19, spectrum A) using the rate constant above confirmed the results of the magnetization transfer experiments.

In order to have a deeper insight of the mechanism of the glycine exchange, the pH dependence of the rate was studied in both H_2O and D_2O in a relatively narrow pH range between 6.5 and 8.5. The line width of the coordinated fluorides increased with decreasing pH in both solvents. In this pH range the external fluoride exchange rate is practically independent of the hydrogen ion concentration; hence, the increase of the line width is

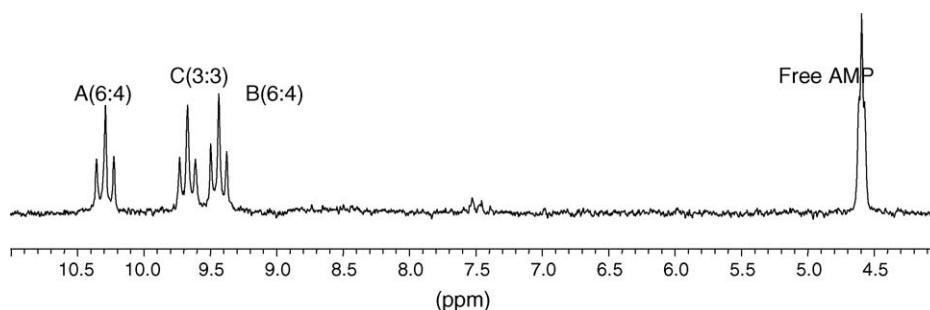


Fig. 20. ^{31}P NMR spectra measured at pH 9.5 in the binary uranium(VI)–AMP system. The triplets indicate the coupling with the neighbouring CH_2 -protons. The signals for the: (A and B) 6:4 complexes and (C) 3:3 complexes [144].

a result of a fast proton catalyzed glycine exchange. A possible mechanism of the exchange is shown in Scheme 8.

The dissociation of fluoride takes place along a separate pathway with the rate constant k_4 . As the coordinated amino group cannot be protonated, the first step in the glycine exchange is the ring opening with a rate constant k_1 . From this ring-opened intermediate the glycine can dissociate without or with protonation of the amino group, followed by the dissociation of the “zwitterion”. A mechanism where the first reaction is much slower than the proton-assisted reaction results in a rate law (Eq. (54)) that is in agreement with the experimental one

$$k_{\text{obs}} = \frac{k_1 k_3 K [\text{H}^+]}{k_{-1} + k_3 K [\text{H}^+]} \quad (54)$$

A plot of $1/k_{\text{obs}}$ versus $1/[\text{H}^+]$ is linear with an intercept $1/k_1$ and a slope $k_{-1}/k_1 k_3 K$. From these quantities the following constants were obtained: $k_1 = 129 \pm 3$ and $143 \pm 2 \text{ s}^{-1}$ and for $k_{-1}/k_3 = K$ $(2.3 \pm 0.1) \times 10^{-9} \text{ M s}$ and $(0.14 \pm 0.02) \times 10^{-9} \text{ M s}$, in H_2O and D_2O , respectively, cf. Table 5. This indicates that the rate constant for the ring opening, k_1 , is independent of the solvent and of the same magnitude as found in the picolinate system. However, the large reverse isotope effect on the subsequent steps in the mechanism is a clear indication of H^+/D^+ bonding to the “free” NH_2 -group.

6.2. Nucleotides

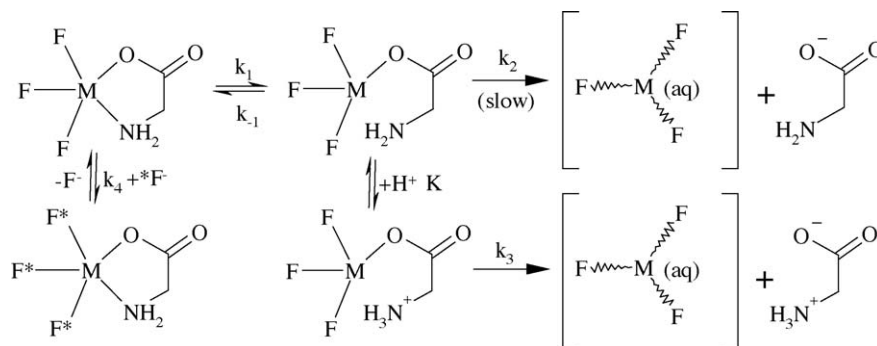
The information-carrying DNA and RNA and related molecules, like nucleotides, are polydentate ligands, with var-

ious potential binding sites, including nitrogen and oxygen donors on the bases, hydroxyl groups on the ribose sugar and negatively charged oxygen atoms in the phosphate group. Depending on external conditions (e.g. pH) and on the size and nature of the metal centre, monodentate or multidentate coordination is possible.

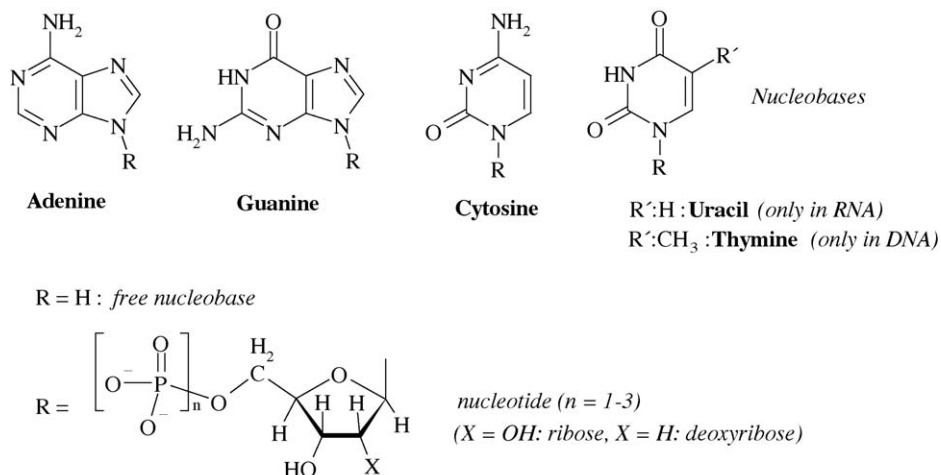
Adenosine, guanosine, cytidine and thymidine are the four most important nucleosides found in nature. They consist of a sugar moiety bound to a heterocycle and are converted to nucleotides upon phosphorylation as shown in Scheme 9.

There are several experimental studies of the interaction between uranium and nucleotides and nucleic acids. A number of them have focused on the application of uranium(VI) as catalyst in the synthesis of 2'-5'-linked oligonucleotides with high regio- and stereoselectivity [126–131]. The UO_2^{2+} -unit polarizes the coordinated ligands strongly, and may enhance the nucleophilicity of the OH groups in a sugar moiety. The coordination of the deprotonated group to uranium will organize the ligands in such a way that inter-nucleotide bond formation from activated nucleotides is promoted and thereby acts as a very effective catalyst in oligonucleotide synthesis.

Another intensively studied field is the application of the uranyl ion as photochemical agent for cleavage of nucleic acids [132–137]. Uranyl-mediated photo-cleavage of nucleic acids is an important method to probe the tertiary structure of DNA and RNA. Although the mechanism of these processes has not yet been fully elucidated, the coordination of the phosphate group to the uranyl ion and the coordination geometry of the formed complexes are of key importance in these reactions.



Scheme 8. Reaction pathways for the exchange of glycinate and fluoride in $\text{UO}_2(\text{glycinate})\text{F}_3^{2-}$ with the free ligands (from Szabó and Grenthe [125], reproduced by the permission of American Chemical Society).



Scheme 9.

The physiological importance of the uranyl–adenosine triphosphate complex was shown 50 years ago [138]. The cellular metabolism is inhibited when uranium replaces Mg(II) from the active ATP–Mg(II)–hexokinase complex, which can therefore not phosphorylate glucose. This observation served as the base for the first study of the complex formation of uranium(VI) with adenine nucleotides by Agarwal and Feldman in the middle of the 1960s [139]. In their pioneering work ¹H NMR spectroscopy was used to study the composition and the structure of the complexes formed in various adenine nucleotide systems.

They suggested the formation of three complexes with adenosine-monophosphate (AMP) at pH above 8: one dimer with uranium to ligand ratio of 2:2 and two others with the ratio 4:2. Later, they re-investigated and modified their originally proposed structure to the one shown in Fig. 21(a) [140].

This proposal has served as a model for other metal–nucleotide complexes with, e.g. molybdenum, and was later cited as “sandwich-type” or “Feldman-complex” [141]. In the middle of 1980s, two research groups re-investigated the uranium(VI) system, using ¹H and ³¹P NMR spectroscopy. Both

confirmed the formation of three uranium(VI)–AMP complexes but one group [142] reported the same structures proposed by Feldman, while the other group proposed the formation of two tetranuclear and one octanuclear complex with hydroxo bridges between the uranyl units [143].

In order to solve the conflict between the different structural proposals Szabó et al. have recently re-investigated the complex formation of uranium(VI) with four nucleotides, adenosine-monophosphate, guanosine-monophosphate (GMP), uridine-monophosphate (UMP) and cytidine-monophosphate (CMP) in the alkaline pH range (8.5–12) by multinuclear NMR spectroscopy [144]. They have found that only two complexes are formed with all ligands in the investigated pH region, independent of the total uranium(VI) and ligand concentrations. The two complexes are inter-converting with pH, and at higher pH (11–12) only one of them exists. Although the coordination of the 5'-phosphate group and the 2'- and 3'-hydroxyl groups of the sugar unit to the uranyl ions are similar to that proposed earlier (“Feldman-complex”), the number and the structures of the complexes are different as determined by a systematic variation

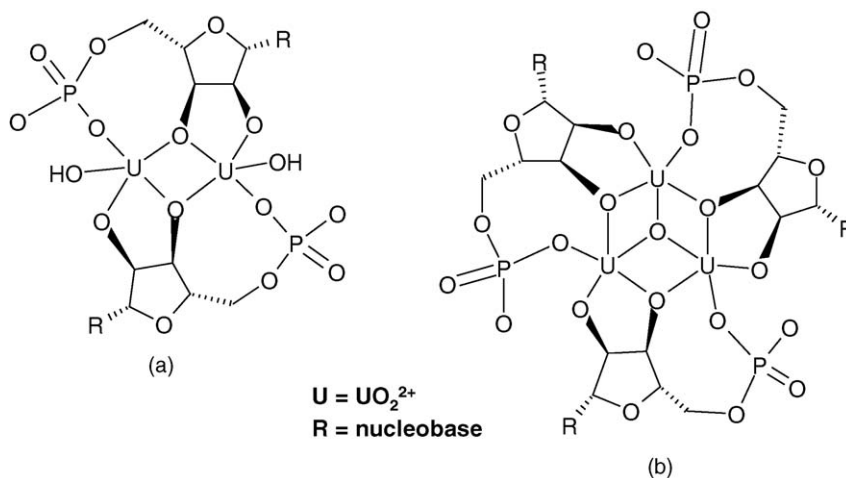


Fig. 21. Structure of the complex formed in the uranium(VI)–AMP system proposed by Feldman (a). The general structure of the complexes formed in the various uranium(VI)–nucleotide monophosphate systems identified by Szabó et al. (b). (U = UO₂²⁺, charges are neglected for simplicity.)

of the ratio of two ligands in ternary uranium(VI)–nucleotide systems. The uranium to nucleotide ratio is 3:3 in one of the complexes as shown in Fig. 21(b), and due to the symmetry gives only one signal in the ^{31}P NMR spectrum as shown in Fig. 20 (signal C).

In the other complex the uranium to ligand ratio is 6:4. It contains two symmetric phosphorous sites, with two phosphorous atoms in each site, which appear as two ^{31}P signals in the NMR spectra (Fig. 20, signals A and B). In the earlier studies, the latter signals were assigned to two different molecules. However, diffusion NMR measurements confirmed that the two signals arising from phosphorous atoms are located in the same molecule.

6.3. Hydroxycarboxylates

Finally, we will discuss the interaction of actinides with ligands containing carboxylate and alcoholic or phenolic hydroxyl groups found in various biological systems. These ligands show high complex forming affinity towards the hard actinide ions. A well-known example is the strong polynuclear complex formation of uranium(VI) with citrate. Citric acid is a common constituent of soils and can also be found in living systems, its complexes with actinide ions can significantly contribute to the speciation and the transportation of these metals in aqueous systems at physiologically or environmentally relevant pH values.

Complex formation with large molecular weight biopolymers possessing these functional groups, like humic and fulvic acids in natural waters, are of key of importance for the migration and immobilization of actinide ions in the environment [145]. Due to the complexity of the structure of the different humic acids the study of their interaction with metal ions is difficult and their complex formation behavior has not been completely understood at the molecular level. The stability constants measured for a given actinide often vary significantly depending

Table 6

log β values for the complexes shown in Scheme 10 where the uncertainty is equal to 3σ ; the data are from [125]

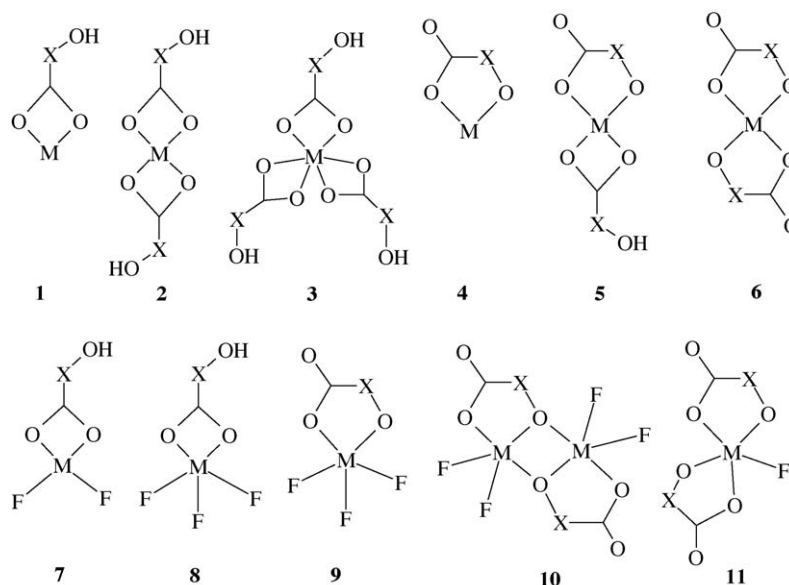
Complex	Glycolate	α -Hydroxyisobutyrate
1	2.38 ^a	3.32 ± 0.02
2	3.95 ^a	5.25 ± 0.02
3	5.16 ^a	6.95 ± 0.03
4	−1.26 ± 0.07	<−2
5	0.19 ± 0.09	0.59 ± 0.03
6	−4.17 ± 0.04	−5.23 ± 0.04
7	10.36 ± 0.09	10.96 ± 0.04
8	11.89 ± 0.10	12.96 ± 0.06
9	5.1 ± 0.10 ^b	–
10	11.09 ± 0.10	–
11	−2.40 ± 0.07	–

^a Literature values.

^b Based on NMR data.

both on the method of preparation, the ionic strength and the experimental technique [145]. Even though several site-binding models exist in the literature, it is generally assumed that carboxylate groups are the primary coordination sites at pH below 8. Nevertheless, other functional groups can also be involved in the complex formation, resulting in different chelate structures as discussed in the following two examples.

Pompe et al. have studied the complex formation behavior of the uranyl ion with natural and chemically modified synthetic humic acids by the aid of time-resolved laser-induced fluorescence spectroscopy [146]. The authors have proved that steric hindrance of the phenol hydroxyl groups by methylation results in a decrease of the degree of the complexation with humic acids; consequently, these groups in humic acids must contribute significantly to the complex formation with uranium(VI) even at pH 4. The authors assumed that the OH groups remain protonated in the complex due to their high pK values. It is well known however that aromatic hydroxyl groups can be deprotonated when



Scheme 10. Structure models of binary and ternary complexes in the uranyl(VI) glycolate and α -hydroxyisobutyrate systems (from Szabó and Grenthe [125], reproduced by the permission of American Chemical Society). M: UO_2^{2+} , X: $-\text{CH}_2-$ (glycolate), $-\text{C}(\text{CH}_3)_2-$ (α -hydroxyisobutyrate).

coordinated to actinide ions, e.g. in complexes with simple phenol ligands; therefore, deprotonation of the aromatic hydroxyl groups in more complicated systems cannot be excluded.

Actinide ions can be mobilized by complex formation with low molecular weight organic compounds, like α -hydroxymonocarboxylates, which can be found in nature as degradation products of humic acids or other organic macromolecules. The alcoholic hydroxyl groups are much weaker acids than aromatic hydroxyl groups, with a pK value in the range 17–20. Examples of deprotonation of the aliphatic OH group upon coordination with metal ions are scarce, with the first example in lanthanide glycolate complexes [147] and a second in uranium(VI) complexes studied by Kakihana et al. [148]. The formation of complexes of this type is expected to have large effects both on the stability constants and the ligand exchange dynamics and on the mobility of actinide ions in natural waters.

Experiments related to the complex formation of Cm(III) and Th(IV) with glycolate have been discussed in Section 2.2. Other examples are provided in a recent study of the complex formation of uranium(VI) with two α -hydroxycarboxylates (glycolate and α -hydroxyisobutyrate) [125]. Based on potentiometric data and various multinuclear NMR spectra the complexes in Scheme 10 could be identified in the studied binary and ternary uranyl–fluoride– α -hydroxycarboxylate systems.

The stoichiometry and the equilibrium constants of the different complexes were determined by potentiometry. Exceptions are the data for $\text{UO}_2(\text{OCH}_2\text{COO})\text{F}_3^{3-}$ and the complexes in the glycine system, which were based on ^{19}F NMR integrals. The equilibrium constants given in Table 6 refer to the following reactions:

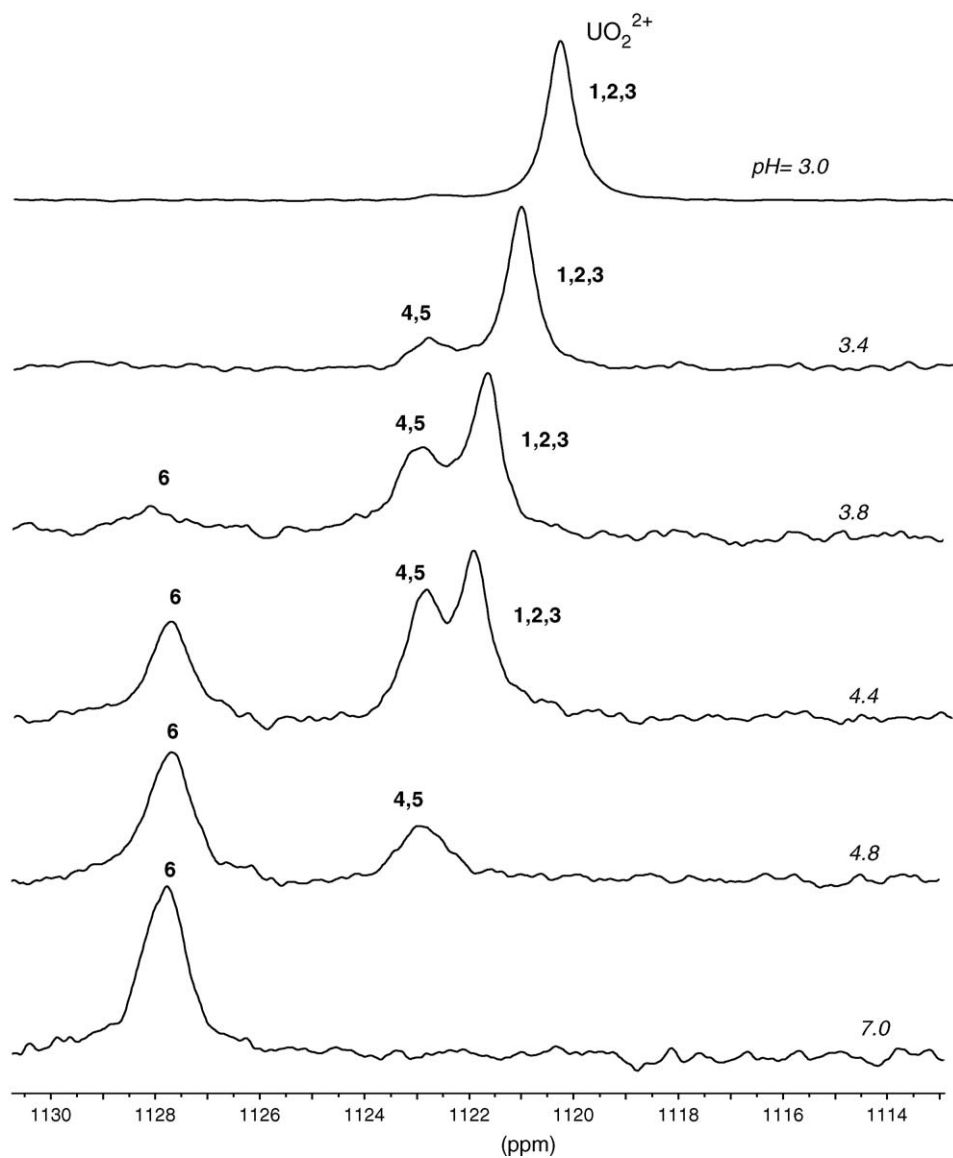
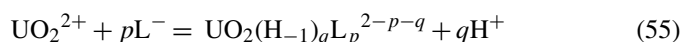
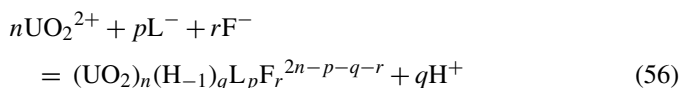


Fig. 22. pH dependence of the ^{17}O NMR spectra measured in the binary U(VI)–glycolate system (54.2 MHz, $[\text{UO}_2^{2+}] = 10$ mM, [glycolic acid] = 50 mM, at 268 K, $[\text{Na}^+] = 1$ M) (from Szabó and Grenthe [125], reproduced by the permission of American Chemical Society). The numbers refer to the structures of the different complexes in Scheme 10.

and



where L^- denotes glycolate or α -hydroxyisobutyrate; for notation see footnote 1.

A comparison of stability constants for the glycolate complexes 1 and 4 indicates a very large increase in the $\text{p}K$ -value for the dissociation of the α -hydroxy proton, from 17 or higher in free glycolate to 3.64 on coordination to uranium(VI), an increase by at least 13 orders of magnitude. At the same time, one can see that the binary α -hydroxyisobutyrate complexes are more stable than the corresponding glycolate complexes at $\text{pH} < 5$ as a result of the inductive effect obtained by replacing the methylene protons in glycolate with methyl groups.

As mentioned before potentiometry cannot distinguish between deprotonation of the OH group in the ligand and from co-ordinated water. This information can be obtained using NMR methods. Such experiments indicate clearly that the α -hydroxycarboxylates are coordinated by only the carboxylate end at lower pH in complexes 1–3, 5, 7 and 8. However, at higher pH separate narrow peaks can be observed for complexes 4–6, in which the α -hydroxycarboxylates are chelated. The narrow line widths of the ^1H and ^{17}O NMR peaks for the chelated complexes in the binary system (4–6) indicate that the coordination and deprotonation of the hydroxyl groups result in a dramatic decrease of the ligand exchange rate, cf Table 5. In complexes in which the glycolate is coordinated by the carboxylate end only (1–3) the glycolate exchange rate is much higher and close to the value measured in the acetate system. For these complexes only one exchange averaged ^{17}O NMR signal can be observed indicating a fast exchange between them (Fig. 22).

In the ternary system the ^{19}F NMR spectra indicate the same large decrease of the ligand exchange rate by increasing the pH. Broad signals can be observed for complexes 7 and 8 as a result of fast glycolate exchange, while narrow peaks appear for the chelate complexes 9–11. For complex 11, three structural isomers with different thermodynamic stability have been identified; the same observations were made in the corresponding picolinate complex (see Fig. 13a). The dimer structure of complex 10 has also been confirmed in solid state by X-ray crystallography [149].

The glycolate exchange reactions have been studied for complexes 6 and 11 using ^1H NMR spectroscopy. The proton signal of the binary complex showed a linear dependence on the free glycolate concentration, from which the second rate order constant of $567 \pm 13 \text{ M}^{-1} \text{ s}^{-1}$ can be calculated. In complex 11, the increase of concentration of the free glycolate had no effect on the signal of the coordinated ligand; therefore, magnetization transfer experiments were used to determine the exchange rate and found to be 1.2 s^{-1} . The fluoride exchange rate is also independent from the free fluoride concentration and the rate measured by magnetization transfer, 12 s^{-1} , is practically the same as found in other ternary systems. These indicate that the fluoride and glycolate exchange in complex 11 follow two parallel and independent pathways (Scheme 4) as was found in the

corresponding ternary oxalate fluoride complex. The experimental data in the glycolate system indicate that a proton catalyzed ring opening is more plausible than a ring opening followed by protonation as observed in the glycine system (Scheme 8). The coordinated oxoacetate has electron pairs available for proton attack and in addition it is a much stronger base than the corresponding glycine complex.

Acknowledgements

This study has been made as a joint project within the EC supported ACTINET network of excellence. Financial support has been obtained through a grant from the Trygger Foundation, the Ministère chargé de la Recherche, Région Nord/Pas de Calais and the Fond Européen de Développement Économique des Régions.

References

- [1] V. Vallet, P. Macak, U. Wahlgren, I. Grenthe, *Theor. Chim. Acta*, in press.
- [2] F.J.C. Rossotti, H. Rossotti, *The Determination of Stability Constants and other Equilibrium Constants in Solution*, McGraw-Hill, New York, 1961.
- [3] (a) M.T. Beck, I. Nagypál, *Chemistry of Complex Equilibria*, Ellis Horwood Ltd., 1990; (b) I. Grenthe, K. Spahiu, A.V. Plyasunov, in: I. Grenthe, I. Puigdomench (Eds.), *Modelling in Aquatic Chemistry*, OECD, Nuclear Energy Agency, Paris, 1997.
- [4] I. Grenthe, J. Varfeldt, *Acta Chem. Scand.* 23 (1969) 988.
- [5] S. Hietanen, L.G. Sillén, *Acta Chem. Scand.* 22 (1968) 265.
- [6] S. Hietanen, *Acta Chem. Scand.* 8 (1954) 1626.
- [7] K.A. Kraus, R.W. Holmberg, *J. Phys. Chem.* 58 (1954) 325.
- [8] C.F. Baes Jr., R.E. Mesmer, *The Hydrolysis of Cations*, Wiley & Sons, New York, 1976.
- [9] T. Stumpf, T. Fanghänel, I. Grenthe, *J. Chem. Soc. Dalton Trans.* (2002) 3799.
- [10] W. Aas, Z. Szabó, I. Grenthe, *J. Chem. Soc. Dalton Trans.* (1999) 1311.
- [11] P. Lubal, J. Havel, *Talanta* 44 (1997) 457.
- [12] P. Lubal, J. Havel, *Chem. Pap.* 51 (1997) 213.
- [13] G. Meinrath, *J. Alloys Compd.* 275–277 (1998) 777.
- [14] G. Meinrath, Y. Kato, T. Kimura, Z. Yoshida, *Radiochim. Acta* 84 (1999) 21.
- [15] J.I. Kim, R. Klenze, H. Wimmer, W. Runde, W. Hauser, *J. Alloys Compd.* 213/214 (1994) 333.
- [16] H. Wimmer, R. Klenze, J.I. Kim, *Radiochim. Acta* 56 (1992) 79.
- [17] R. Klenze, P. Panak, J.I. Kim, *J. Alloys Compd.* 271–273 (1998) 746.
- [18] W. Aas, E. Steinle, T. Fanghänel, J.I. Kim, *Radiochim. Acta* 84 (1998) 85.
- [19] T. Fanghänel, H.T. Wegener, T. Könecke, V. Neck, P. Paviet-Hartmann, E. Steinle, J.I. Kim, *Radiochim. Acta* 82 (1998) 47.
- [20] T. Fanghänel, J.I. Kim, *J. Alloys Compd.* 271–273 (1998) 728.
- [21] G. Geipel, A. Brachmann, V. Brendler, G. Bernhard, H. Nitsche, *Radiochim. Acta* 75 (1996) 199.
- [22] G. Geipel, G. Bernhard, V. Brendler, H. Nitsche, *Radiochim. Acta* 82 (1998) 59.
- [23] H. Moll, G. Geipel, V. Brendler, G. Bernhard, H. Nitsche, *J. Alloys Compd.* 271–273 (1998) 765.
- [24] H. Moll, G. Geipel, T. Reich, G. Bernhard, Th. Fanghänel, I. Grenthe, *Radiochim. Acta* 91 (2003) 11.
- [25] I. Billard, K. Lützenkirchen, *Radiochim. Acta* 91 (2003) 285.
- [26] C. Moulin, P. Decambox, V. Moulin, J.G. Decaillon, *Anal. Chem.* 67 (1995) 348.

- [27] W.D. Horrocks Jr., V.K. Arkle, F.J. Liotta, D.R. Sudnick, *J. Am. Chem. Soc.* 105 (1983) 3455.
- [28] Z. Fazekas, T. Yamamura, H. Tomiyasu, *J. Alloys Compd.* 271–273 (1998) 756.
- [29] I. Billard, E. Ansoborlo, K. Apperson, S. Arpigny, M.E. Azenha, D. Birch, P. Bros, H.D. Burrows, G. Choppin, L. Coustou, V. Dubois, Th. Fanghänel, G. Geipel, S. Hubert, J.I. Kim, T. Kimura, R. Klenze, A. Kronenberg, M. Kumke, G. Lagarde, G. Lamarque, S. Lis, C. Madic, G. Meinrath, C. Moulin, R. Nagaishi, D. Parker, G. Planckue, F. Scherbaum, E. Simoni, S. Sinkov, C. Viallesoubranne, *Appl. Spectrosc.* 57 (2003) 1027.
- [30] G. Geipel, M. Acker, D. Vulpius, G. Bernhard, H. Nitsche, Th. Fanghänel, *Spectrochim. Acta Part A* 60 (2004) 417.
- [31] T. Toraiishi, N. Aoyagi, S. Nagasaki, S. Tanaka, *Dalton Trans.* 21 (2004) 3495.
- [32] N. Aoyagi, T. Toraiishi, G. Geipel, H. Hotokezaka, S. Nagasaki, S. Tanaka, *Radiochim. Acta* 92 (2004) 589.
- [33] I. Billard, A. Rustenholz, L. Sémon, K. Lützenkirchen, *Chem. Phys.* 270 (2001) 345.
- [34] J.R. Lakowicz, *Principles of Fluorescence Spectroscopy*, Plenum Press, New York, 1983.
- [35] (a) C. Madic, D.E. Hobart, G.M. Begun, *Inorg. Chem.* 22 (1983) 1494; (b) D.A. Palmer, C. Nguyen-Trung, *J. Solution Chem.* 24 (1995) 1282.
- [36] Z. Szabó, W. Aas, I. Grenthe, *Inorg. Chem.* 36 (1997) 5369.
- [37] V. Vallet, U. Wahlgren, I. Grenthe, *J. Am. Chem. Soc.* 125 (2003) 14941.
- [38] G. Johansson, *Pure Appl. Chem.* 12 (1988) 1773.
- [39] C. Den Auwer, E. Simoni, S. Conradson, C. Madic, *Eur. J. Inorg. Chem.* (2003) 3843.
- [40] V. Vallet, Z. Szabó, I. Grenthe, *J. Chem. Soc. Dalton Trans.* (2004) 3799.
- [41] A.L. Ankudinov, S.D. Conradson, J. Mustre de Leon, J.J. Rehr, *Phys. Rev. B* 57 (1998) 7518.
- [42] J.-P. Blaudeau, S.A. Blaudeau, Z.A. Zygumt, L.A. Curtiss, D.T. Reed, B.E. Bursten, *Chem. Phys. Lett.* 310 (1999) 347.
- [43] M.R. Antonio, L. Soderholm, C.W. Williams, J.-P. Bladeau, B.E. Bursten, *Radiochim. Acta* 89 (2001) 1.
- [44] P.G. Allen, J.J. Bucher, D.K. Shuh, N.M. Edelstein, T. Reich, *Inorg. Chem.* 36 (1997) 4676.
- [45] J.H. Matonic, B.L. Scott, M.P. Neu, *Inorg. Chem.* 40 (2001) 2638.
- [46] Th. Kowall, P. Caravan, H. Bourgeois, L. Helm, F.P. Rotzinger, A.E. Mehrbach, *J. Am. Chem. Soc.* 120 (1998) 6569.
- [47] W. DeW. Horrocks, D.R. Sudnick, *J. Am. Chem. Soc.* 101 (1979) 334.
- [48] T. Kimura, G.R. Choppin, *J. Alloys Compd.* 213/214 (1994) 313.
- [49] G. Johansson, *Acta Chem. Scand.* 22 (1968) 399.
- [50] G. Johansson, M. Magini, H. Ohtaki, *J. Solution Chem.* 20 (1991) 775.
- [51] H. Moll, M.A. Denecke, M.A.F. Jalilvand, M. Sandström, I. Grenthe, *Inorg. Chem.* 38 (1999) 1795.
- [52] T. Yang, S. Tsushima, A. Suzuki, *Chem. Phys. Lett.* 360 (2002) 534.
- [53] T. Yang, S. Tsushima, A. Suzuki, *J. Solid State Chem.* 171 (2003) 235.
- [54] (a) S. Tsushima, T. Yang, Y. Mochizuki, Y. Okamoto, *Chem. Phys. Lett.* 375 (2003) 204; (b) S. Tsushima, T. Yang, *Chem. Phys. Lett.* 40 (2005) 68.
- [55] S.D. Conradson, *Appl. Spectrosc.* 52 (1998) 252.
- [56] V. Vallet, T. Privalov, U. Wahlgren, I. Grenthe, *J. Am. Chem. Soc.* 126 (2004) 7766.
- [57] V. Vallet, U. Wahlgren, B. Schimmelpfennig, Z. Szabó, I. Grenthe, *J. Am. Chem. Soc.* 123 (2001) 11999.
- [58] S. Spencer, L. Gagliardi, N.C. Handy, A.G. Ioannou, C.-K. Skylaris, A. Willets, *J. Phys. Chem. A* 103 (1999) 1831.
- [59] P.J. Hay, R.L. Martin, G. Schreckenbach, *J. Phys. Chem. A* 104 (2000) 6259.
- [60] P. Guilbaud, G. Wipff, *J. Phys. Chem. A* 97 (1993) 5685.
- [61] M. Åberg, D. Ferri, J. Glaser, I. Grenthe, *Inorg. Chem.* 32 (1983) 3986.
- [62] J. Neufeind, L. Soderholm, S. Skanthakumar, *J. Phys. Chem. A* 108 (2004) 2733.
- [63] T. Toraiishi, I. Farkas, Z. Szabó, I. Grenthe, *J. Chem. Soc. Dalton Trans.* (2002) 3805.
- [64] T. Toraiishi, I. Grenthe, *J. Chem. Soc. Dalton Trans.* (2003) 1634.
- [65] D. Ferri, I. Grenthe, F. Salvatore, *Inorg. Chem.* 22 (1983) 3162.
- [66] J. Bruno, I. Grenthe, P. Robouch, *Inorg. Chim. Acta* 158 (1989) 221.
- [67] (a) D.L. Clark, S.D. Conradson, D.W. Keogh, P.D. Palmer, B.L. Scott, C.D. Tait, *Inorg. Chem.* 37 (1998) 2893; (b) D. Rai, A.R. Felmy, N.J. Hess, D.A. Moore, M.A. Yui, *Radiochim. Acta* 82 (1998) 17.
- [68] S. Voliotis, A. Rimsky, *Acta Cryst. B* 31 (1975) 2612.
- [69] S. Voliotis, A. Rimsky, *Acta Cryst. B* 31 (1975) 2615.
- [70] (a) I. Grenthe, J. Fuger, R.J.M. Konings, R.J. Lemire, A.B. Mueller, C. Nguyen-Trung, H. Wanner, *Chemical Thermodynamics of Uranium*, North-Holland, 1992; (b) R. Guillaumont, T. Fanghänel, J. Fuger, I. Grenthe, V. Neck, D.A. Palmer, M.H. Rand, *Update on the Chemical Thermodynamics of Uranium, Neptunium, Plutonium, Americium and Technetium*, North-Holland, 2003.
- [71] R.J. Lemire, J. Fuger, H. Nitsche, P. Potter, M.H. Rand, J. Rydberg, K. Spahiu, J.C. Sullivan, W.J. Ullman, P. Vitorge, H. Wanner, *Chemical Thermodynamics of Neptunium and Plutonium*, North-Holland, 2001.
- [72] T.I. Docrat, J.F.W. Mosselmans, J.M. Charnock, M.W. Whitley, D. Collison, F.R. Livens, C. Jones, M.J. Edmiston, *Inorg. Chem.* 38 (1999) 1879.
- [73] D.L. Clark, S.D. Conradson, S.A. Ekberg, N.J. Hess, M.P. Neu, P.D. Palmer, W. Runde, C.D. Tait, *J. Am. Chem. Soc.* 118 (1996) 2089.
- [74] L. Gagliardi, I. Grenthe, B.O. Roos, *Inorg. Chem.* 40 (2001) 2976.
- [75] A.F. Wells, *Structural Inorganic Chemistry*, Oxford University Press, 1990.
- [76] T.C.W. Mak, W.H. Yip, *Inorg. Chim. Acta* 109 (1985) 131.
- [77] V. Vallet, U. Wahlgren, B. Schimmelpfennig, H. Moll, Z. Szabó, I. Grenthe, *Inorg. Chem.* 40 (2001) 3516.
- [78] D.L. Clark, S.D. Conradson, R.J. Donohue, W.D. Keogh, D.E. Morris, P.D. Palmer, R.G. Rogers, C.D. Tait, *Inorg. Chem.* 38 (1999) 1456.
- [79] U. Wahlgren, H. Moll, I. Grenthe, B. Schimmelpfennig, L. Maron, V. Vallet, O. Gropen, *J. Phys. Chem. A* 103 (1999) 8257.
- [80] V. Vallet, U. Wahlgren, Z. Szabó, I. Grenthe, *Inorg. Chem.* 41 (2002) 5626.
- [81] H. Moll, T. Reich, Z. Szabó, *Radiochim. Acta* 88 (2000) 411.
- [82] I. Infante, L.J. Vischer, *Comput. Chem.* 25 (2004) 386.
- [83] G. Schreckenbach, P.J. Hay, R.L. Martin, *Inorg. Chem.* 37 (1998) 4442.
- [84] V. Vallet, H. Moll, U. Wahlgren, Z. Szabó, I. Grenthe, *Inorg. Chem.* 42 (2003) 1982.
- [85] J. Vázquez, C. Bo, J.P. Poblet, J. De Pablo, J. Bruno, *Inorg. Chem.* 42 (2003) 6136.
- [86] U. Cosentino, A. Villa, D. Pitea, G. Moro, V. Barone, A. Maiocchi, *J. Am. Chem. Soc.* 124 (2002) 4901.XX.
- [87] S.F. Lincoln, *Pure Appl. Chem.* 51 (1979) 2059.
- [88] H. Tomiyasu, H. Fukutomi, *Bull. Res. Lab. Nucl. Reactors* 7 (1982) 57.
- [89] K.L. Nash, J.C. Sullivan, *J. Alloys Compd.* 271–273 (1998) 712.
- [90] Z. Szabó, J. Glaser, I. Grenthe, *Inorg. Chem.* 35 (1996) 2036.
- [91] J.I. Friese, K.L. Nash, M.P. Jensen, J.C. Sullivan, *Radiochim. Acta* 89 (2001) 35.
- [92] Y. Ikeda, S. Soya, H. Fukutomi, H. Tomiyasu, *J. Inorg. Nucl. Chem.* 41 (1979) 1333.
- [93] N. Bardin, P. Rubini, C. Madic, *Radiochim. Acta* 83 (1998) 189.
- [94] I. Farkas, I. Bányai, Z. Szabó, U. Wahlgren, I. Grenthe, *Inorg. Chem.* 39 (2000) 799.
- [95] Y. Ikeda, H. Tomiyasu, H. Fukutomi, *Bull. Res. Lab. Nucl. Reactors* 4 (1979) 47.
- [96] Y. Ikeda, H. Tomiyasu, H. Fukutomi, *Inorg. Chem.* 23 (1984) 1356.
- [97] (a) C. Clavaguéra-Sarrio, V. Brenner, S. Hoyau, C.J. Marsden, P. Millié, J.-P. Dognon, *J. Phys. Chem. B* 107 (2003) 3051; (b) C. Clavaguéra, R. Pollet, J.M. Soudan, V. Brenner, J.-P. Dognon, *J. Phys. Chem. B* 109 (2005) 7614.

- [98] (a) P. Guilbaud, G. Wipff, *J. Phys. Chem.* 97 (1993) 5685;
(b) P. Guilbaud, G. Wipff, *J. Inclusion Phenom. Mol. Recognit.* 16 (1993) 169;
(c) P. Guilbaud, G. Wipff, *J. Mol. Struct. (Theochem.)* 366 (1996) 55;
(d) P. Guilbaud, G. Wipff, *New J. Chem.* 20 (1996) 631;
(e) F. Hutschka, A. Dedieu, L. Troxler, G. Wipff, *J. Phys. Chem. A* 102 (1998) 3773;
(f) D. Hagberg, G. Karlström, B.O. Roos, L. Gagliardi, *J. Am. Chem. Soc.* 127 (2005) 14250.
- [99] A. Chaumont, G. Wipff, *Inorg. Chem.* 43 (2004) 5891;
A. Chaumont, E. Engler, G. Wipff, *Inorg. Chem.* 42 (2003) 5348.
- [100] C. Den Auwer, D. Guillaumont, P. Guilbaud, S.D. Conradson, J.J. Rehr, A. Ankudinov, E. Simoni, *New J. Chem.* (2004) 929.
- [101] (a) T. Ziegler, *J. Chem. Soc. Dalton Trans.* (2002) 642;
(b) T. Ziegler, *J. Autschbach, Chem. Rev.* 105 (2005) 2695.
- [102] P. Macak, unpublished results.
- [103] T. Toraiishi, T. Privalov, B. Schimmelpfennig, U. Wahlgren, I. Grenthe, *J. Phys. Chem. A* 107 (2003) 9456.
- [104] Z. Szabó, I. Grenthe, *Inorg. Chem.* 37 (1998) 6214.
- [105] E. Brücher, J. Glaser, I. Toth, *Inorg. Chem.* 30 (1991) 2239.
- [106] D.L. Clark, D.E. Hobart, M.P. Neu, *Chem. Rev.* 95 (1995) 25.
- [107] V. Frei, H. Wendt, *Ber. Der Bunsen-Ges.* 74 (1970) 593.
- [108] K. Mizouka, I. Grenthe, Y. Ikeda, *Inorg. Chem.* 44 (2005) 4472.
- [109] R.G. Wilkins, *Chemical Kinetics and Mechanism of Reactions of Transition Metal Complexes*, second ed., VCH, 1991.
- [110] M.J. Kendrick, M.T. May, M.J. Plishka, K.D. Robinson, *Metals in Biological Systems*, Ellis Horwood, Chichester, 1992.
- [111] F. Ciardelli, E. Tsuchida, D. Wöhrle (Eds.), *Macromolecule–Metal Complexes*, Springer, Berlin, 1996.
- [112] J.R. Duffield, D.M. Taylor, D.R. Williams, in: K.A. Gschneidner Jr., L. Eyring (Eds.), *Handbook on the Physics and Chemistry of Rare Earths, Lanthanides/Actinides: Chemistry*, vol. 18, North Holland, 1994, p. 591 (Chapter 129).
- [113] J.R. Duffield, D.M. Taylor, in: A.J. Freeman, C. Keller (Eds.), *Handbook on the Physics and Chemistry of the Actinides*, vol. 4, Elsevier Science Publisher B.V., Amsterdam, 1986 (Chapter 4).
- [114] A. Bismondo, U. Castellani, S. Sitran, *Inorg. Chim. Acta* 110 (1985) 205.
- [115] A. Raghavan, M. Santappa, *J. Inorg. Nucl. Chem.* 35 (1973) 3363.
- [116] H. Wieczorek, H. Kozłowski, *Inorg. Nucl. Chem. Lett.* 16 (1980) 401.
- [117] M.M. Khalil, M. Taha, *Monatsh. Chem.* 135 (2004) 385.
- [118] M. Khodari, *Mikrochim. Acta* 131 (1999) 231.
- [119] K. Kangaraj, V.V. Ramanujam, *J. Inorg. Nucl. Chem.* 39 (1977) 489.
- [120] N. Nourmand, N. Meissami, *Polyhedron* 1 (1982) 537.
- [121] P.V. Selvaraj, M. Santappa, *J. Inorg. Nucl. Chem.* 39 (1977) 119.
- [122] A. Bismondo, L. Rizzo, *Thermochim. Acta* 196 (1992) 131.
- [123] N.C. Li, B.E. Doody, J.M. White, *J. Am. Chem. Soc.* 79 (1957) 5859.
- [124] H. Huang, S. Chaudhary, J.D. van Horn, *Inorg. Chem.* 44 (2005) 813.
- [125] Z. Szabó, I. Grenthe, *Inorg. Chem.* 39 (2000) 5036.
- [126] H. Sawai, K. Kuroda, T. Hojo, *Bull. Chem. Soc. Jpn.* 62 (1989) 2018.
- [127] H. Sawai, T. Shibusawa, K. Kuroda, *Bull. Chem. Soc. Jpn.* 63 (1990) 1776.
- [128] M. Shimazu, K. Shinozuka, H. Sawai, *Angew. Chem. Int. Ed. Engl.* 32 (1993) 870.
- [129] H. Sawai, H. Katsutaka, K. Kuroda, *J. Chem. Soc. Perkin Trans.* (1992) 505.
- [130] H. Sawai, T. Ito, K. Kokaji, M. Shimazu, K. Shinozuka, H. Taira, *Bioorg. Med. Chem. Lett.* 6 (1996) 1785.
- [131] H. Sawai, A. Hirano, H. Mori, K. Shinozuka, B. Dong, R.H. Silverman, *J. Med. Chem.* 46 (2003) 4926.
- [132] P.E. Nielsen, C. Jeppesen, O. Buchardt, *FEBS Lett.* 235 (1988) 122.
- [133] A.R. Hill Jr., L.E. Orgel, *Bioconjugate Chem.* 2 (1991) 431.
- [134] P.E. Nielsen, C. Hiort, S.H. Sönnichsen, O. Buchardt, O. Dahl, B. Nordén, *J. Am. Chem. Soc.* 114 (1992) 4967.
- [135] P.E. Nielsen, N.E. Møllegaard, *J. Mol. Recognit.* 9 (1996) 228.
- [136] S.H. Sönnichsen, P.E. Nielsen, *J. Mol. Recognit.* 9 (1996) 219.
- [137] D. Wittberger, C. Berens, C. Hammann, E. Westhof, R. Schroeder, *J. Mol. Biol.* 300 (2000) 339.
- [138] I. Feldman, J. Jones, R. Cross, *J. Am. Chem. Soc.* 89 (1967) 49.
- [139] R.P. Agarwal, I. Feldman, *J. Am. Chem. Soc.* 90 (1968) 6635.
- [140] I. Feldman, K.E. Rich, *J. Am. Chem. Soc.* 91 (1969) 4559.
- [141] C.F.G.C. Geraldes, M.M.C.A. Castro, *J. Inorg. Biochem.* 28 (1986) 319.
- [142] M.M.C.A. Castro, C.F.G.C. Geraldes, *Inorg. Chim. Acta* 140 (1987) 377.
- [143] M. Kainosho, M. Takahashi, *Nucl. Acid Res. Symp. Ser.* 12 (1983) 181.
- [144] Z. Szabó, I. Furró, I. Csöreg, *J. Am. Chem. Soc.* 127 (2005) 15236.
- [145] G.R. Choppin, B. Allard, in: A.J. Freeman, C. Keller (Eds.), *Handbook on the Physics and Chemistry of the Actinides*, vol. 3, Elsevier Science Publisher B.V., Amsterdam, 1986 (Chapter 11).
- [146] S. Pompe, K. Schmeide, M. Bubner, G. Geipel, K.H. Heise, G. Bernhard, H. Nitsche, *Radiochim. Acta* 88 (2000) 553.
- [147] I. Grenthe, *Acta Chem. Scand.* 23 (1969) 1253.
- [148] M. Kakahana, T. Nagumo, M. Okamoto, H. Kakahana, *J. Phys. Chem.* 91 (1987) 6128.
- [149] I. Farkas, I. Csöreg, Z. Szabó, *Acta Chem. Scand.* 53 (1999) 1009.